AD NUMBER

AD238120

NEW LIMITATION CHANGE

TO

Approved for public release, distribution unlimited

FROM

Distribution authorized to U.S. Gov't. agencies and their contractors; Administrative/Operational use; 6 Jan 1960. Other requests shall be referred to Air Force Cambridge Research Labs, Hanscom AFB MA.

AUTHORITY

AFCRL, ltr, 3 Nov 1971

(10)

AFCRC-TN-60-364

TRG-121-SR-1

CONTRACT NO. AF19(604)-3476
SCIENTIFIC REPORT NO. 1

YAGI ANTENNA STUDY

The research reported in this document has been sponsored by the Electronics Research Directorate of the Air Force Cambridge Research Center, Air Research and Development Command, under Contract No. AF19(604)-3476. The publication of this report does not necessarily constitute approval by the Air Force of the findings or conclusions contained herein.

January 6, 1960

Alan F. Kay
Author

Lawrence Goldmantz
Approval

TRG, Incorporated
2 Aerial Way
Syosset, N. Y.

TECHNICAL RESEARCH GROUP

"Requests for additional copies by Agencies of the Department of Defense, their contractors and other Government agencies should be directed to the:

ARMED SERVICES TECHNICAL INFORMATION AGENCY
ARLINGTON HALL STATION
ARLINGTON 12, VIRGINIA

Department of Defense contractors must be established for ASTIA services or have their 'need-to-know' certified by the cognizant military agency of their project or contract."

"All other persons and organizations should apply to the:

U.S. DEPARTMENT OF COMMERCE
OFFICE OF TECHNICAL SERVICES
WASHINGTON 25, D.C."

TABLE OF CONTENTS

ABSTRACT

An experimental study of the near fields of yagis was undertaken. Quantities measured were the surface wave phase velocity, longitudinal and transverse field decay; excitation efficiency, tolerance effects, ohmic losses, and behavior near the source. Particular emphasis is given to long maximum gain yagis (up to 300λ in length) and how the above quantities enter to limit the gain. A partially empirical theory is developed from the extensive measured data which gives a simple picture of the fields around a yagi suitable for computing far field patterns without the errors of the Hansen-Woodyard theory. This theory should be applicable to other parasitic linear, endfire antennas.

I. INTRODUCTION

Dielectric rods [1], yagis (arrays of short, parallel rods or pins) [2], cigars (arrays of parallel discs) [3], and many other similar structures support a surface wave with phase velocity slower than light. It will be convenient here to give such structures a collective name, and the acronym PLASER (Parasitic Linear Antenna Surface-wave Endfire Radiation) suggests the distinguishing features. When fed at one end, parasitically (as distinguished from an array of elements each "actively" fed) a PLASER supports a surface wave which will radiate an endfire beam unless the structure is modulated or loaded in special ways which we will not consider here. The word 'linear' is used to rule out two dimensional structures such as a dielectric-clad ground plane or a "fakir's bed," which is the planar analogue of the yagi.

PLASERS have often been designed in the past on the basis of the Hansen-Woodyard condition [4]. This states that the optimum length ℓ for maximum gain G is given by

$$\ell = \frac{\pi}{\beta - k}, \quad k = \frac{2\pi}{\lambda} \tag{1}$$

where β and k are the surface wave and free space propagation constants, respectively, and further that

$$G = 7.2 \frac{\ell}{\lambda} . \tag{2}$$

The "gain per wavelength" which is 7.2 for a Hansen-Woodyard design, is a convenient figure of merit for PLASERS. One conclusion that follows immediately from these results is that for high gain, long PLASERS are required, supporting "fast" slow waves, ones for which β is close to k.

Although the Hansen-Woodyard theory is correct for uniformly illuminated active endfire arrays,* it has been shown to be definitely in error for PLASERS [2]. Optimum lengths appear to be somewhat shorter than that given by (1) and the maximum gains so far achieved are almost twice the value of (2) for short PLASERS ($\ell \simeq 1\lambda$) increasing to about half the value of (2) for long PLASERS ($\ell \simeq 100\lambda$).

The Hansen-Woodyard theory is based on the concept that radiation is due entirely to a uniform surface wave traveling the length of the line source. This picture is not correct for yagis as pointed out in [2]. Data taken by Ehrenspeck and Poehler showed that the surface wave amplitude (as measured along a reference line parallel to the yagi axis as close to the axis as the yagi structure permits) is not uniform. The study in [2] was confined to yagis six wavelengths or less in length, and to the fairly slow surface waves which are optimum for these lengths. The phase and amplitude plots shown in [2] give a fairly satisfying picture of the mechanism of launching and establishing the surface wave for such yagis. Also the techniques for

* By "active endfire array" is meant an array in which the phase and amplitude of each element is controlled by means of an individual connection to a feeding transmission line, rather than by parasitic excitation.

maximizing gain as described in [2] appear adequate for short yagis. The present paper is primarily concerned with the problem of maximizing gain for longer yagis and in consideration of the faster surface waves which are used on them.

There is no theoretical limit to gain per wavelength if supergaining is permitted. For active endfire line sources the relationship between gain and Q can be deduced from previous analysis for broad side line sources [5]. If excessively high Q's are not allowed, one is led to the semi-quantitative practical limitation on the maximum gain per wavelength of about 10 for ℓ large compared to λ. It is not clear whether very long PLASERS could achieve this value. The possibility exists that ohmic losses in practical structures, practical tolerance limitations, or difficulty in exciting a sufficiently "fast" slow wave efficiently, might impose a more severe ceiling on the gain per wavelength than the theoretical supergaining limitations.

The research reported in this paper was undertaken to study this question of limitations on gain of long PLASERS. Pertinent to this question is the mechanism of the excitation and formation of the surface wave on the PLASER. This becomes clear if we consider a hypothetical situation. Suppose a slow wave whose propagation constant β is close to the free space value k, that is, a "fast" slow wave, can be efficiently and fully established close to the source i.e. at a distance ℓ much less than

$\pi/(\beta-k)$. Assume the PLASER is terminated at that point. Since a "fast"slow wave looks very much like a plane wave over a large area and since it is not closely bound to the structure it will radiate with little reflection to produce a narrow pencil beam. It is shown in [12] that, as (1) and (2) imply, the resulting gain will be inversely proportional to $\beta-k$ when $\beta-k$ is small. Under these hypotheses we have "created" a supergain antenna. If the surface wave can be efficiently excited without supergaining, therefore it apparently must take a length of the order of ℓ given by (1) to fully establish itself. Thus in order to answer properly the question of what limits the gain per wavelength of long PLASERS, we have had to determine how the surface wave is launched and established, and why the length is required in the first place. For this purpose we have studied experimentally the near fields of various PLASER configurations.

II. APPARATUS

The photograph (Figure 1) shows a 3 ft by 32 ft aluminum ground plane in which a row of pins is embedded to form a yagi about 300λ in length. The pins are $.2\lambda$ apart (λ=1.2992") and are right circular brass cylinders of diameter .062" $\pm$.0005" and height above the ground plane L which is variable by means of an adjustable support strip running the length of the yagi below the ground plane. At the bottom left is visible an open waveguide (RG 52/U) source. Other sources were occasionally employed as described later.

It is convenient to think of cylindrical(r,θ,z) coordinates

FIGURE 1

"300 λ Yagi"

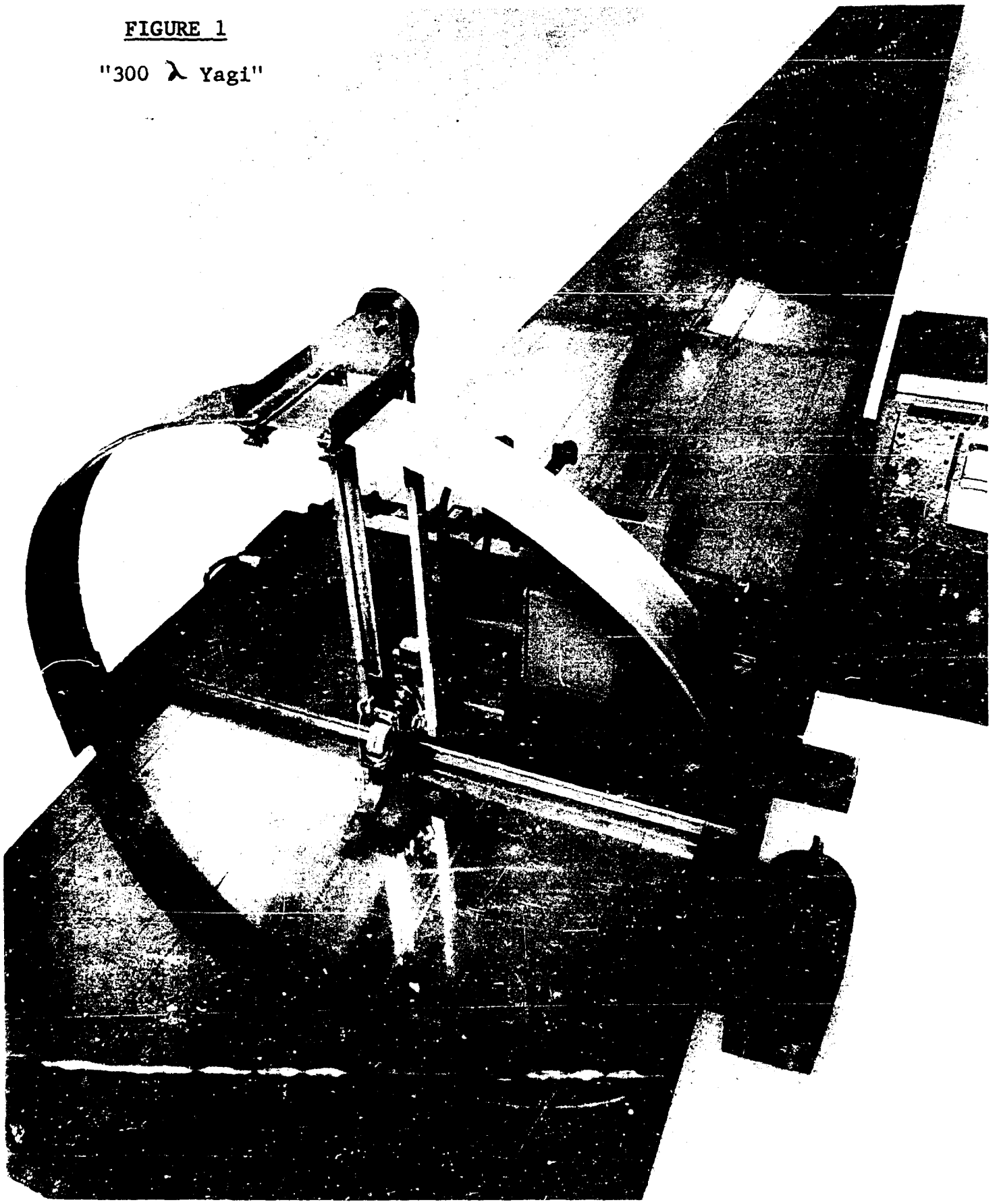

with the z axis coincident with the yagi axis, the source at the origin, and the half space above the ground plane described by $0 \leq \theta \leq \pi$. The carriage shown in the photograph was designed to support an open waveguide probe to take field measurements in the z or θ directions. The carriage was geared to a synchro transmitter which operated a chart drive for recording amplitude and (with the help of a bridge circuit) phase versus either the longitudinal (z) or transverse (θ) probe motion. For all the measurements described herein the ground plane is effectively infinite and the yagi semi-infinite. Scattering by the receiving probe or carriage was usually negligible as could be determined by judicious use of absorbing material. It will often be helpful to adopt the point of view that the yagi here is an open transmission line and the source is a lossy transition from the closed waveguide transmission line to the open surface wave transmission line. By an open transmission line is meant one whose exterior transverse boundary condition is the radiation condition in contradistinction to the closed transmission line with a finite metallic wall boundary condition. A few of the measurements reported here were also made on short yagis ($\ell \simeq 5$ to 10λ) in free space.

III. THEORETICAL FIELD ON AN INFINITE PLASER, LOWEST ORDER MODE

In an infinite dielectric rod supporting a lowest order "dipole mode" surface wave [1] each field component exterior to the dielectric is proportional to

(3) $$(c_0 K_0(kXr) + c_1 K_1(kXr))e^{-j\beta z}$$

where

(4) $$\beta = k\sqrt{1+X^2}$$

and c_0 and c_1 depend only on the angle θ and the particular field component under consideration. In the case of a planar surface wave, the field components are of the form

(5) $$e^{-j\beta z - kXy}$$

where y is the height above the surface. Equation (4) also holds here too. The quantity X has the further significance in the planar TM case that it is the normal reactance of the surface normalized with respect to the characteristic impedance of free space. In the case of the PLASER we continue to call X the "reactance" although the physical significance of this terminology is no longer obvious.

The infinite yagi may be analyzed without considering a boundary value problem in such a way as to show that its field dependence is similar to the dielectric rod dipole mode. Since the result will be required to identify the surface wave in our field measurements, we give the derivation here. It may also be of some general interest to show

how much of the character of the electromagnetic field can be determined without solving any boundary value problem.

Imagine an infinite array of pins along the z-axis in free space with centers located at $z = nd$, $n = 0, \pm 1, \pm 2, \ldots$, and oriented with the pin axes parallel to the x axis. Consider the field at a general point P in space given in cylindrical coordinates by (r, θ, z). The total field at P is the sum of the fields due to the currents in all the pins. Let us assume the current on the nth pin equals $I_0 e^{-j\beta nd}$ for all n. Our assumption therefore, is that the pin currents are those due to excitation by a uniform surface wave with propagation constant $\beta = k\sqrt{1+X^2}$. We shall also assume that each pin radiates like an infinitesimal electric dipole with axis parallel to x and dipole moment p_0 and that $r >> \frac{\lambda}{2\pi}$ so that the point P is in the far field of all the dipoles.

FIGURE 2 - SPATIAL RELATIONSHIPS

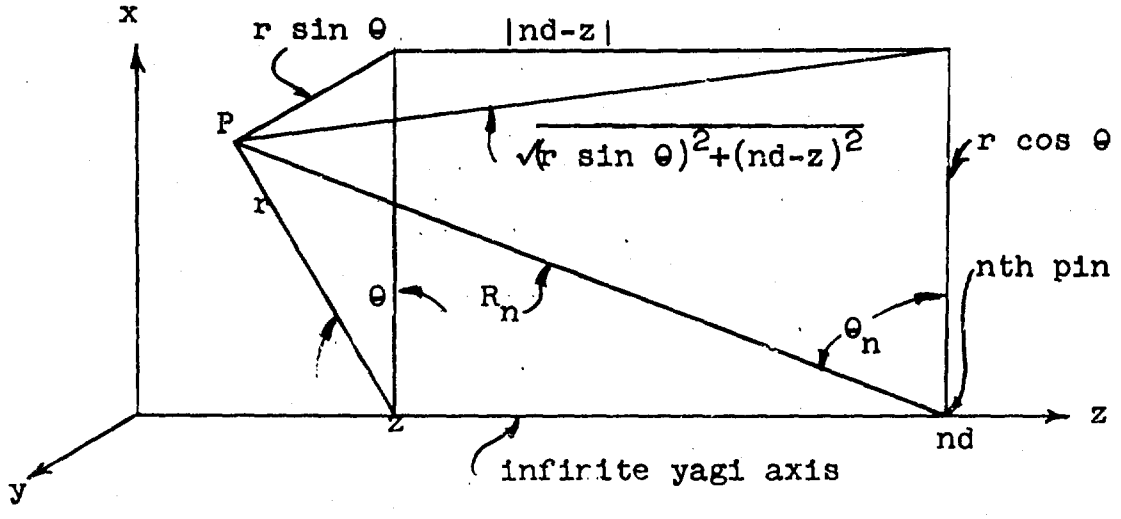

The x component of the E field at P can be obtained by superposition of the well-known dipole far fields. It must in fact be equal to

$$(6) \qquad E_x(P) = \frac{p_0 k^2}{4\pi\epsilon_0} \sum_{n=-\infty}^{\infty} e^{-j\beta\, nd}\, \frac{e^{ikR_n}}{R_n} \sin^2\theta_n$$

where

$$(7) \qquad \sin\theta_n = \frac{\sqrt{(r\sin\theta)^2+(nd-z)^2}}{R_n}, \quad R_n = \sqrt{r^2+(nd-z)^2}\ .$$

Let us consider the case $\theta = \frac{\pi}{2}$, which simplifies because $\theta_n = \frac{\pi}{2}$. Then by the Poisson summation formula [7]

$$(8) \qquad \frac{4\pi\epsilon_0}{k^2 p_0} E_x(P) = \sum_{n=-\infty}^{\infty} \frac{e^{-j(-\beta\, nd + k\sqrt{r^2+(nd+z)^2})}}{\sqrt{r^2+(nd+z)^2}}$$

$$= \sum_{m=-\infty}^{\infty} \int_{-\infty}^{\infty} \frac{e^{-j(k\sqrt{r^2+(td-z)^2} + \beta td)}}{\sqrt{r^2+(td-z)^2}} e^{-2m\pi jt}\, dt$$

$$= \frac{2}{d} \sum_{m=-\infty}^{\infty} K_0\left(r\sqrt{(\beta+\tfrac{2m\pi}{d})^2-k^2}\right) e^{-j(\beta+\frac{2m\pi}{d})z}, \qquad (\theta = \tfrac{\pi}{2})$$

where $K_0(x)$ is the modified Hankel function of the second kind of order zero. If

$$(9) \qquad \beta < \frac{2\pi}{d} - k, \quad (\beta > k)$$

the arguments of all of the modified Hankel functions are positive and there will be no radiating mode. If d is sufficiently small (e.g. for $\beta \simeq k$, if $d < \frac{\lambda}{2}$) then only the $m = 0$ mode is important, all others being exponentially small compared to it. In this case,

$$(10) \qquad E_x(P) \simeq \frac{k^2}{2\pi\epsilon_0 d} K_0(kXr) e^{-jk\sqrt{1+X^2}z} .$$

In so far as this approximation is valid, the field is θ independent since the right member of (10) is the unique solution of the scalar wave equation which has the appropriate behavior at infinity and takes on the boundary values in the plane $\theta = \pm \frac{\pi}{2}$ which are given by the right member of (10). Measurements indicated that E_x is the only appreciable component of E at least for "fast" slow waves. (In the case: X = .097, L = .169", no polarization component orthogonal to E_x exceeded 33 db below peak E_x at any point). If then we assume that E_y and E_z are negligible, the relation $\nabla \times E = -j\omega\mu H$ implies that the only significant component of H is H_y and that the ratio E_x/H_y, the surface wave longitudinal impedance, is a constant $Z_0/\sqrt{1+X^2}$.

When we compare this result with our experimental results, several points must be kept in mind;

(a) the waveguide probe couples also to the horizontal H field which is

$$(11) \qquad H_y(P) = \sum_{n=-\infty}^{\infty} \frac{e^{-j(\beta\, nd + k\sqrt{r^2+(nd-z)^2})}(nd-z)}{r^2+(nd-z)^2} \,.$$

However, with the same validity as the approximation in (10) we have seen that the coupling to $H_y(P)$ has the same r,z, and θ dependence as the right member of (10).

(b) the measured currents on the pins are not uniform but have a decreasing amplitude the further the pins are from the source (the phase does follow $e^{-j\beta z}$ closely, however).

(c) there are only a finite number of pins.*

IV. GENERAL NATURE OF THE FIELD ABOVE A SEMI-INFINITE YAGI AND RELATIONS BETWEEN THE PRINCIPLE MEASURED PARAMETERS

For orientation purposes it will be helpful to anticipate the results described in detail in later sections and to divide the space around the yagi into five regions as shown in Figure 3. Although the boundaries between regions are not physically sharp, the field has distinctive characteristics in each region.

(1) "near field cylinder" The cylinder, whose equation is $r \sim \frac{\lambda}{4}$, is excluded from our considerations for four reasons:

a) it contains the pins themselves and is approximately the region of the near field of the individual

---

* It is of interest to observe that one can estimate how many pins of uniform current amplitude are required to produce a field which looks like a pure surface wave by estimating how many terms are required to sum the series in (6) with a certain accuracy.

FIGURE 3

THE FIVE REGIONS OF SPACE ABOVE A YAGI

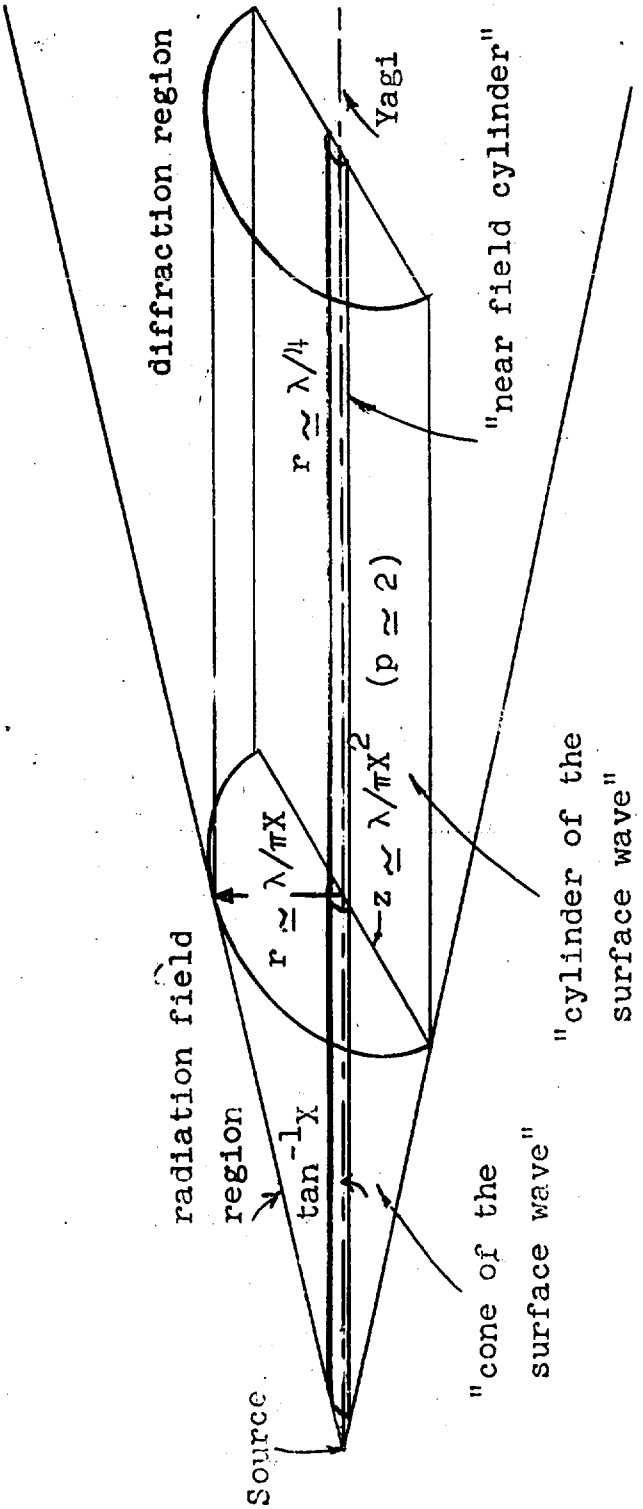

pins, which was excluded in the theory of the preceding section.

b) yagi-probe coupling makes it difficult to interpret measurements made inside this cylinder.

c) a complete picture can be obtained from measurements made in the other regions.

d) the region is sufficiently small so that its presence may usually be neglected.

(2) "cylinder of the surface wave" This is the region in which the surface wave is "fully established." The field is virtually that of the infinite surface wave. Any variation in the field from eq (8) is due to pin or ground plane tolerances, any attenuation is due to ohmic losses, primarily of the currents in the pins. Approximately

$$\frac{\int_0^{\lambda/\pi X} K_0^2(kXr)\,r\,dr}{\int_0^{\infty} K_0^2(kXr)\,r\,dr} = 97.4\% \tag{12}$$

of the total surface wave energy is contained theoretically in this cylinder. The boundary of this cylinder is $r = \lambda/\pi X$ and it is much larger than the near field cylinder, in all cases of practical interest.

(3) "cone of the surface wave" In this region the field has the phase and transverse amplitude dependence of the pure surface wave. However, the longitudinal amplitude dependence is not uniform but decays with respect to "z". This is the region in which the surface wave becomes established. It is convenient to introduce the

normalized distance

(13) $$p = kzX^2 .$$

We shall show that the cone of the surface wave ends and the surface wave is fully established somewhere between $p = 1$ and $p = 2\pi$ depending on the criterion used. In order to keep a sense of proportion it should be noted that for optimum gain, a short uniform yagi [2] should be terminated when $p \simeq 4.5$ $(\ell \simeq .7\frac{\lambda}{X^2})$, while the Hansen-Woodyard length is $p \simeq 2\pi$.

It is probably not a coincidence that p equals in magnitude the "Sommerfeld numerical distance" for the plane earth [8]. The criterion for an observation point on the surface to be in the far field of a source for both the yagi and the plane earth is $p >> 1$. The connecting link between the two problems is the plane reactive surface or fakir's bed, in which the significance of p can be demonstrated with essentially the same analysis as in the flat earth problem. The connection between the yagi and the fakir's bed is an empirical one, which we have observed, that the field in the vertical plane of a yagi is not much different from that above fakir's bed with the same reactance and source.

(4) <u>"the radiation field region"</u> The field in this region is largely unaffected by the presence of the yagi. It has the inverse square dependence on distance from the source and the spherical phase front characteristic of a radiation

field. The angular pattern dependence is similar to the pattern of the source in free space. The region is defined by the inequality $r > Xz$.

(5) "the diffraction region" This is the region between the cylinder of the surface wave and the radiation field region.

V. EXPERIMENTAL VERIFICATION OF THE FUNDAMENTAL SURFACE WAVE PARAMETERS

Phase Velocity $\beta = 2\pi/\lambda_g$

The phase velocities of the faster surface waves with which we are concerned are extremely close to the velocity of light and require an accurate determination to distinguish the difference. The measurement technique was as follows: A shorting plate, creating a standing wave, was moved along the yagi through many periods of the standing wave. The plate rested on the ground plane and had a small slot for the pins to pass through. The standing wave periods were detected by a probe in a slotted line behind the feed. The distance the plate moved was carefully measured and λ_g was then determined as this distance divided by half the number of periods. The experiment was repeated several times and the results averaged. The frequency had to be held to 1 part in 10^5 to obtain meaningful results. The shorting plate had to be large enough to give a high enough VSWR for accurate determination of the periodicity. Preliminary measurements showed also that the short could not be too large or moved too close to the source otherwise unduly small values of λ_g would be observed. Later the criterion was determined

that the short must not extend into the radiation field region. The resulting values of λ_g and X for the fastest waves are shown in Table 1. Note that the "crude" value of free space wavelength at this frequency, $\lambda = 1.3000"$, is not accurate enough for a meaningful determination of X.

TABLE 1

Pin Height L	λ_g(in.)	$X = \sqrt{(\frac{\lambda}{\lambda_g})^2 - 1}$ (λ = 1.2992 in)	Excitation efficiency η of open waveguide source
.169"±.005"	1.2931	.097	.195
.144"±.005"	1.2982	.040	.050

Excitation Efficiency

The excitation efficiency η is defined as the ratio of the power radiated into the surface wave to the total power radiated by the source. It was determined as follows: The source was tuned to a VSWR less than 1.05. The input power P_0 to the source was established as a reference from a calibrated directional coupler and a relative power detecting unit consisting of a matched bolometer detector and a standing wave amplifier. An open waveguide probe identical to the source, was located at some point in the "cylinder of the surface wave," a distance z from the source, in the same position with respect to the pins as the source. The relative power received P_1 was observed by a power detection unit calibrated against that used to monitor the transmitted power. If it is assumed that multiple scattering between the source and probe, either via free space or via the surface wave, is negligible, then

(14) $$P_1 = P_0 e^{-2\alpha z} T_{12} T_{21}$$

where T_{12} is the power transmission coefficient of the junction between the open and closed transmission lines (equal, by reciprocity, to T_{21}), and α is the attenuation of the surface wave in nepers per unit z. By definition

(15) $$\eta = T_{12} = T_{21}$$

so that η may be determined from a measurement of P_1/P_0, α, and z.

For fast slow waves, multiple scattering has been found negligible but, in any case, the effect of multiple scattering can be largely eliminated by averaging P_1 over a distance of $\lambda_g/2$. As a check on this measurement technique, the Deschamps moving short method [9] was also used a number of times. The latter method gives also the complete scattering matrix of the junction at the cost of a more elaborate procedure. Results were about the same in both cases.

We observed only a slight dependence of excitation efficiency on the source provided the source was small, centered on the pins, and polarized vertically. Comparative results for various sources are given in Table 2. With all these sources, and some others such as a V feed having parameter values scaled from [10], the excitation efficiency depends primarily on the reactance and not on the source.

TABLE 2a

Excitation Efficiency of Various Sources

(Pin spacing .260" in all cases. Pin height L is shown f = 9.085 kmc unless otherwise specified)

L	f(kmc)	Source S_1	S_2	S_5
.260	11	.62	.79	.77
.260	11.5	.57	.68	.725
.260	12.0	.46	.50	.64

TABLE 2b

S_3 center height above top of pins	η, for L = .230"
-.120"	.46
-.060"	.48
0	.49
+.060"	.55
+.120"	.53

Source S_5: η = .63

TABLE 2c

L	S_4	S_5
.169"	.168	.195

Source Code Letters

S_1: open waveguide, .4" x .9" aperture } tested with yagis with no ground plane

S_2: small horn, .9" x .9" aperture }

S_3: resonant slot in an "infinite" vertical ground plane, .062" x .620" } tested with yagi on ground plane

S_4: stub source
stub height .305"
reflector height .300"
stub reflector spacing .260" } tested with yagi on ground plane

S_5: open waveguide, .4" x .9" aperture

Ohmic Losses

Ohmic losses were determined by measuring the field variation with respect to z with the probe immediately over the pins within the cylinder of the surface wave. A very accurate reading for the low loss cases could be obtained by a probe travel over the whole 300λ yagi if necessary. By recording the continuous variation of field strength, a best fitting exponential attenuation (straight line on a db plot) eliminates errors due to multiple reflections between source and probe via the surface wave, tolerance variations, and occasional spurious room reflections. A typical plot of this type is shown in Figure 4.

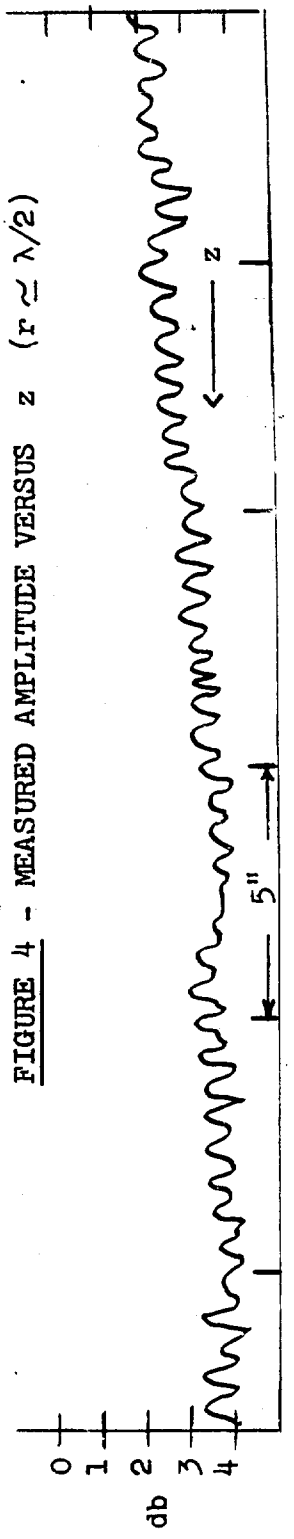

FIGURE 4 - MEASURED AMPLITUDE VERSUS z ($r \simeq \lambda/2$)

Ohmic losses were found not to be important for fast slow waves. For example over the length 300λ with L = .144" the diminution in the surface wave amplitude attributable to ohmic losses was not greater than 1 db. The ohmic loss A in db/λ increases as L increases, and above pin heights of L = .185", where reliable measurements could be made, A is such that over a

Hansen-Woodyard length array (ℓ given by eq (1), or $\ell \simeq \lambda/X^2$) the total loss remains approximately independent of ℓ at about .4 db. Figure 5a extends the data of Table 1 to greater pin heights. Figure 5b shows the frequency dependence at a fixed pin height. Figure 5c is data similar to that of Figure 5a except that the pin spacing has been increased to .4λ. Figures 5d, e, and f are data on entirely different yagi structures, the latter two - S band. With any given structure and element spacing we have found that there is a maximum reactance obtainable as a function of the element height. We call these the "cut-off reactance" and "cut-off" heights. Figure 5a and 5c illustrate that if one compares pin heights for the same reactance, the principal effect of increasing pin spacing is an increase in the sharpness of the "cut-off" pin height and a decrease in the "cut-off reactance." This is also illustrated in Figure 5f where the element spacing was the smallest used, .13λ. This structure supported the maximum yagi reactance we have yet measured, X = 1.6. Below the cut-off, for a given X there is little difference between η or A for the two cases of Figure 5a and 5c. The η , X relationship as indicated in these figures is almost independent of the yagi structure and as previously mentioned, the source. However the attenuation is associated with the large currents on the pins when they are near resonant length.

Figure 5d is for a brass disc-on-rod or "cigar" structure. The rod diameter was .140", the disc thickness and

Note: A, η, and X plotted on same vertical scale.

EXCITATION EFFICIENCY η, REACTANCE X, AND OHMIC LOSS A IN db/λ FOR VARIOUS STRUCTURES

FIGURE 5a

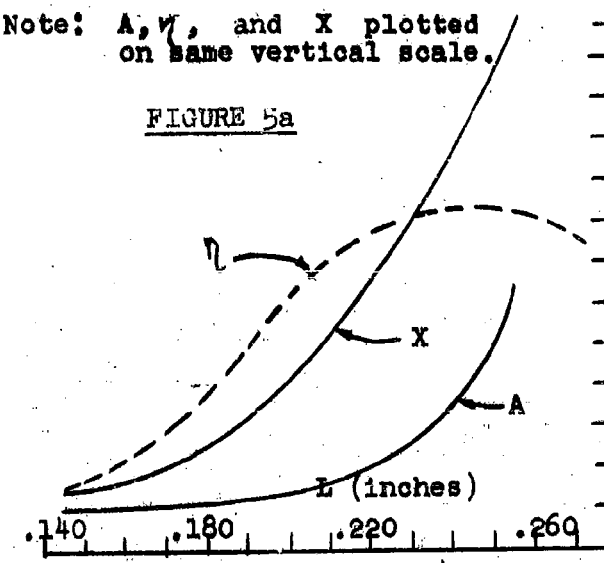

FIGURE 5b

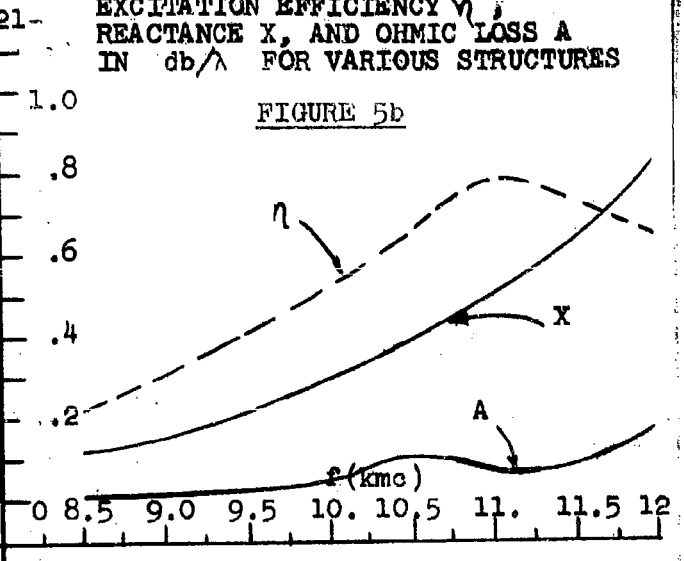

FIGURE 5c

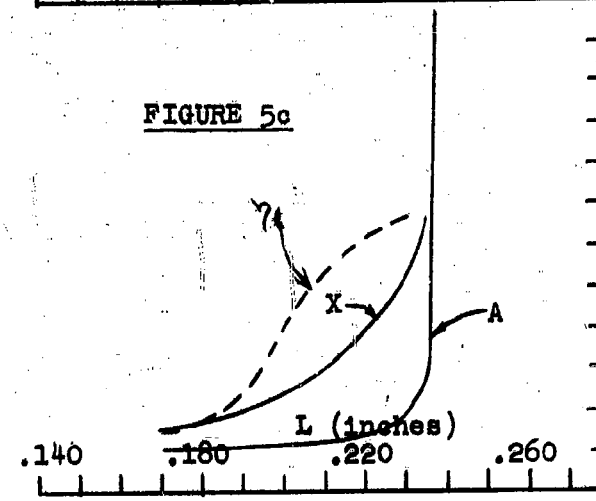

X BAND CIGAR

FIGURE 5d

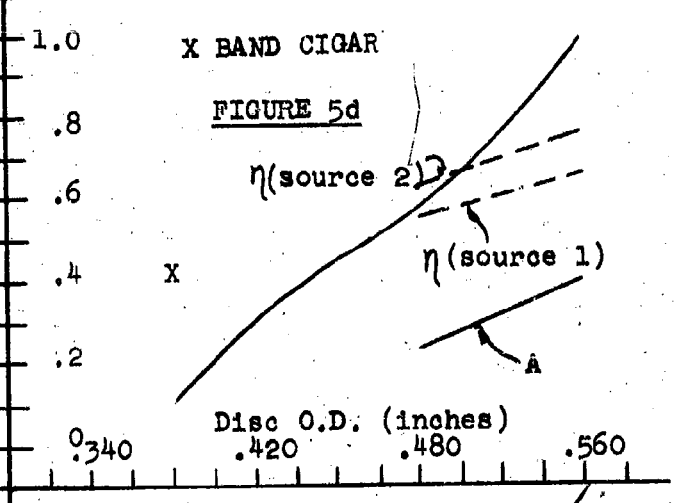

S BAND PRINTED YAGI - GLASS EPOXI

f = 3100 mc

FIGURE 5e

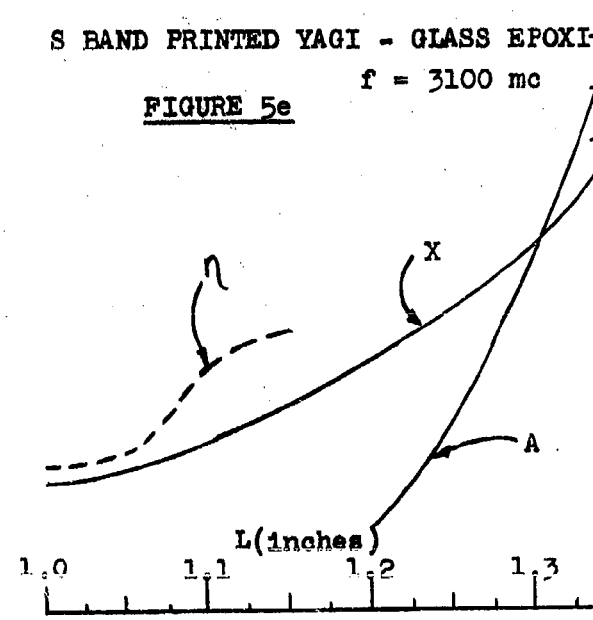

S BAND PRINTED YAGI - TEFLON GLAS

f = 3100 mc

FIGURE 5f

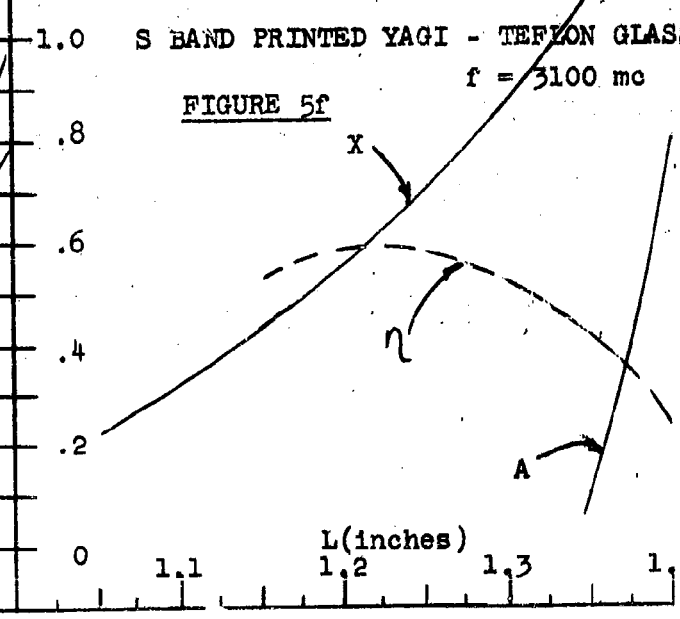

spacing were .031" and .260". The reactance was varied by varying the disc outer diameter as shown.

The S band yagi (Figure 5e) was made of 1/16" glass-epoxi printed circuit board, clad on one side with 2 oz. copper. The dipole widths were .25" and spacing 1.00". This structure was tested without a ground plane, that is, in free space. Comparing equivalent reactances, the attenuation in this yagi is about four times (in db) that of the pin yagis. Most of this difference can be attributed to the loss in the dielectric accompanying large dipole currents. Figure 6f is for a similar structure except that the dielectric is low-loss teflon glass and the element spacing has been reduced by half.

Besides spacing the elements closer together, the performance of the pin structures in regard to ohmic losses can be improved by two different techniques, as illustrated in Figure 6:

(1) silver plating the pins (2) use of a yagi element with lower resonant Q. Figure 6 shows that the db loss with pins of diameter 1/8" is about one-third that of the 1/16" diameter pins. While this is not particularly important for yagi design it is important for the design of surface wave lenses. The reactance of a surface wave Luneberg lens is unity at the center and may require ray paths of many wavelengths near this high reactance, so that only very low loss structures would be suitable.

FIGURE 6

ATTENUATION IN YAGIS SHOWING EFFECT OF SILVER PLATING AND DECREASED ELEMENT Q.

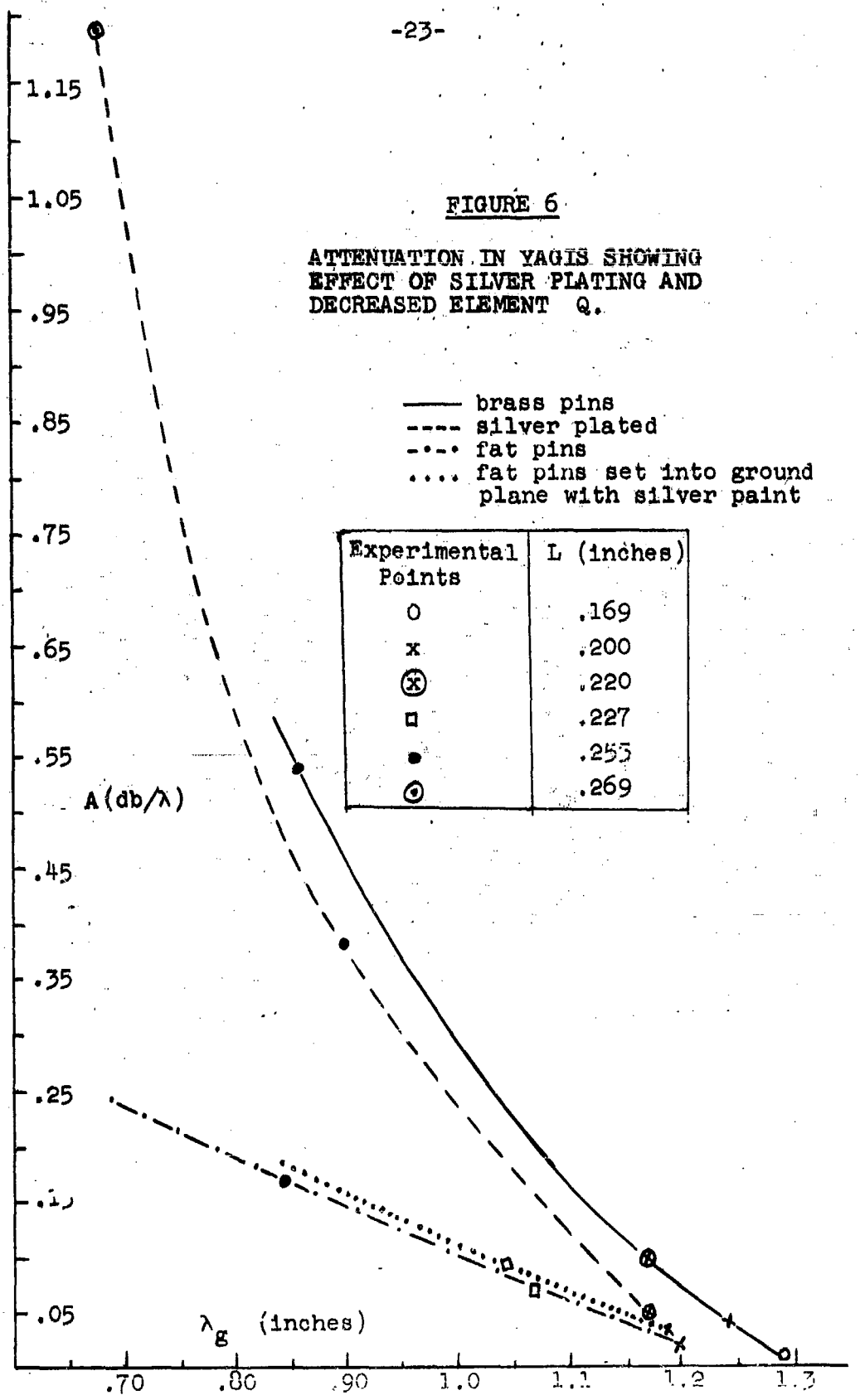

VI. PHASE FRONT MEASUREMENTS

Figures 7, 8, and 9 show measured phase versus r for several values of z at pin heights L = .144", .169", and .185". The first two of these plots were taken with $\Theta = \pi/2$ (vertical plane), the latter with $\Theta = 0$ (horizontal plane). Since the field is almost independent of Θ, this difference is not significant. The case $\Theta = 0$ was usually employed after it was learned that the resulting data was smoother in that case, probably because the effect of ground plane irregularities is minimized when both source and probe are on the surface.

We observe from the measured data that the plane phase front of the surface wave is formed only close to the yagi where the propagation constant is that of the surface wave, the previously measured β. Away from the yagi, the phase front is spherical and travels with the free space propagation constant k. There is no discontinuity in the phase front if p is not large compared to one.

These observations suggest the following empirical theory valid for values of p which are not large compared to one: <u>the surface wave exists inside a cone centered on the source with axis along the yagi and vertex half angle equal to $\tan^{-1}\chi$.</u> The detailed reasoning is as follows: Let A be the point where the spherical and plane phase fronts meet, at a distance r_0 from the yagi. The rays $\overrightarrow{SA}$ and $\overrightarrow{SB}$ of Figure 10 are drawn from a source to the same phase front. Therefore the phase delays from S to A and from S to B must be equal. The energy on SA

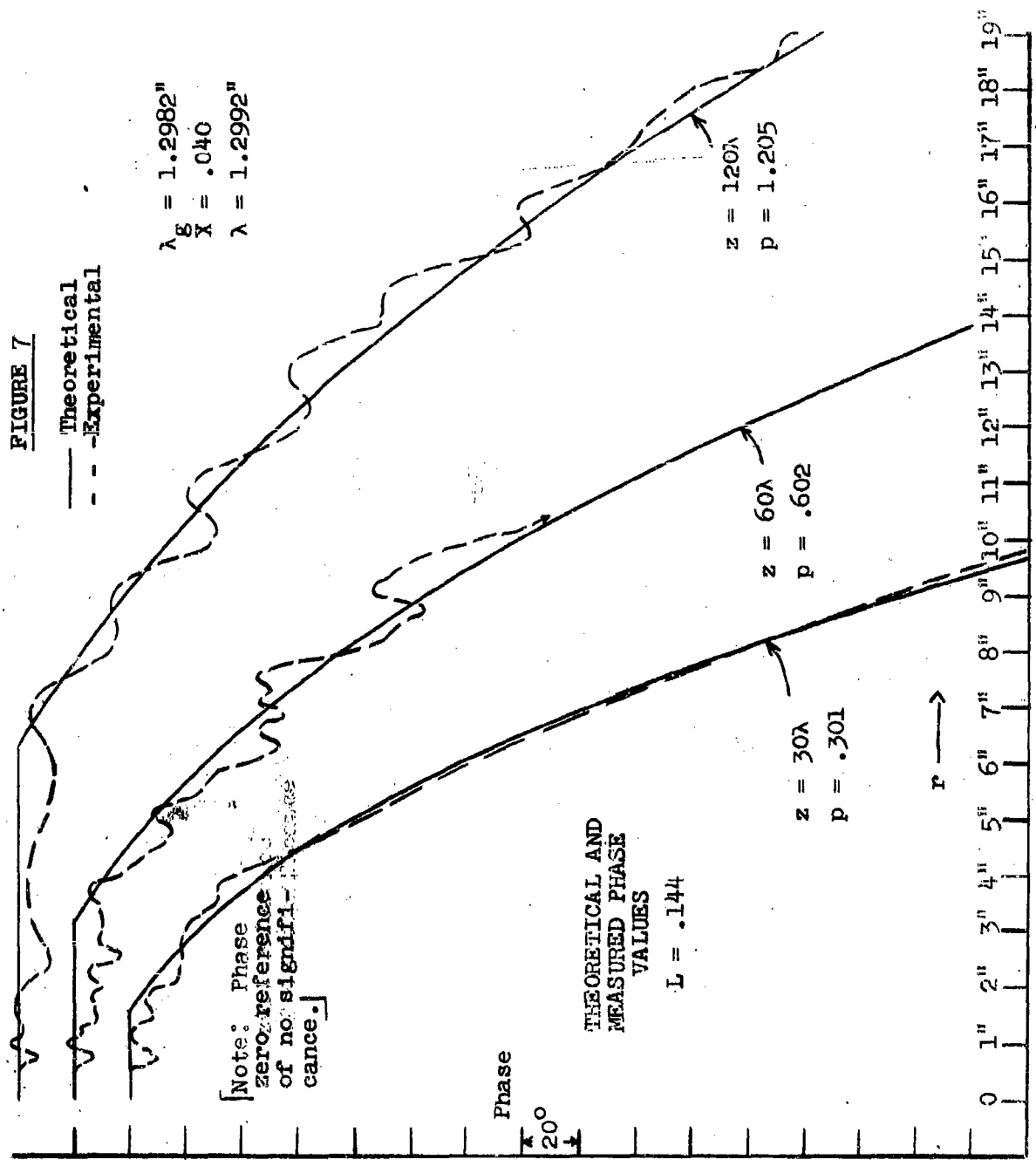
FIGURE 7
Theoretical
Experimental
λ_g = 1.2982"
$\bar{\lambda}$ = .040
λ = 1.2992"
z = 120λ
p = 1.205
z = 60λ
p = .602
z = 30λ
p = .301
THEORETICAL AND MEASURED PHASE VALUES
L = .144
Note: Phase zero reference of no significance.
Phase
20°
r
0 1" 2" 3" 4" 5" 6" 7" 8" 9" 10" 11" 12" 13" 14" 15" 16" 17" 18" 19"

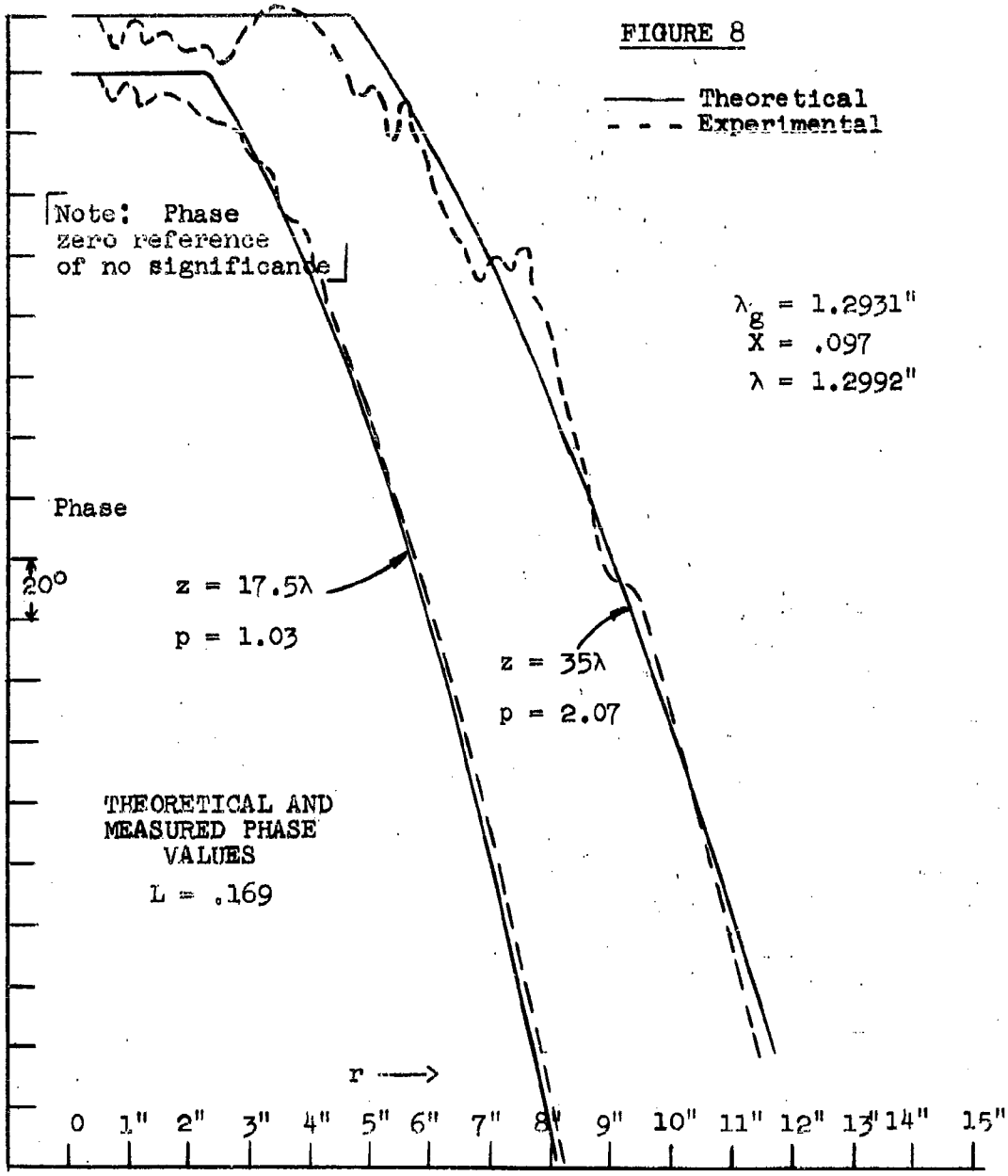
FIGURE 8
Theoretical
Experimental
Note: Phase zero reference of no significande
λ_g = 1.2931"
X = .097
λ = 1.2992"
Phase
20°
z = 17.5λ
p = 1.03
z = 35λ
p = 2.07
THEORETICAL AND MEASURED PHASE VALUES
L = .169
r
0 1" 2" 3" 4" 5" 6" 7" 8" 9" 10" 11" 12" 13" 14" 15"

FIGURE 9

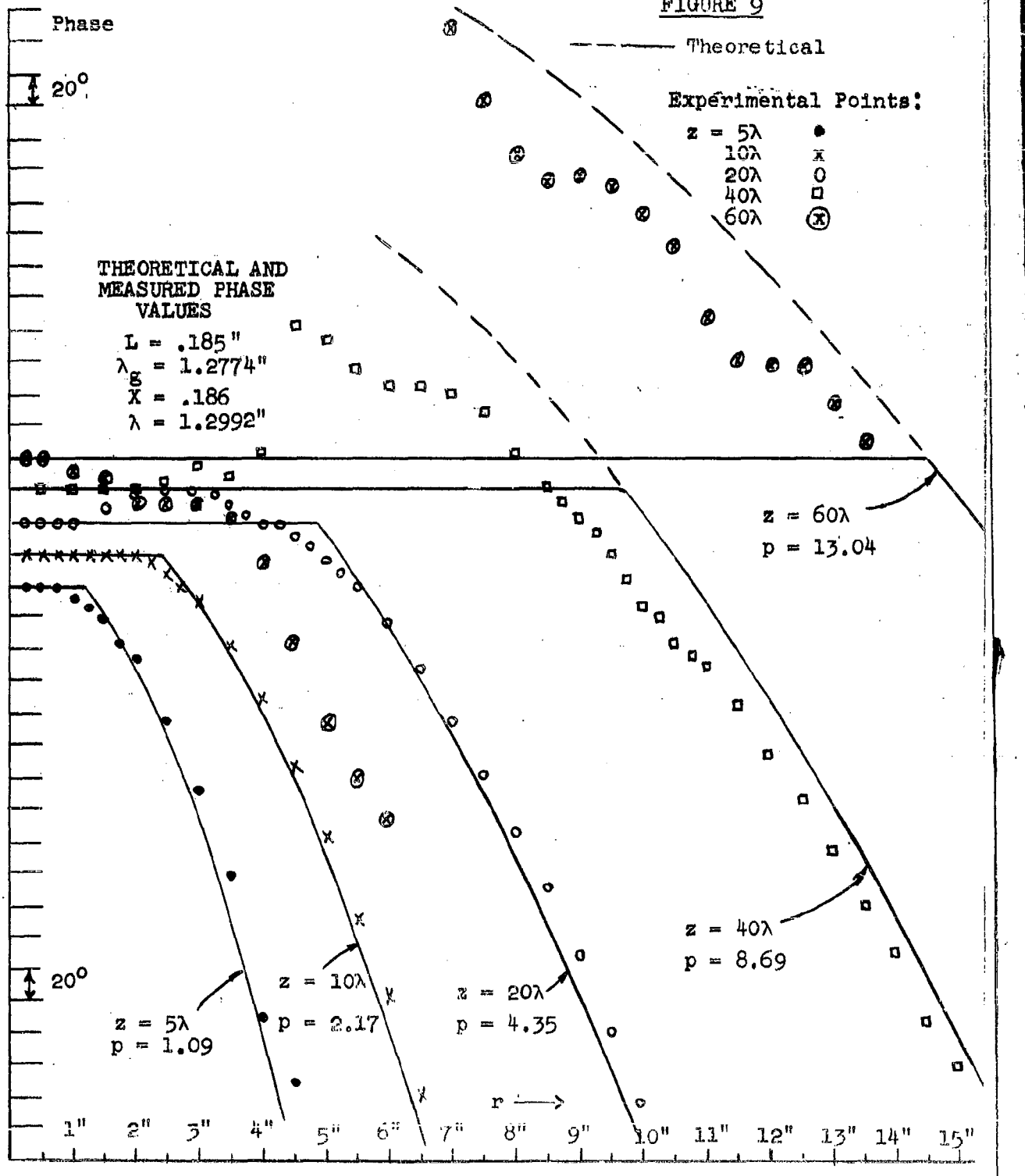
Phase
20°
Theoretical
Experimental Points:
z = 5λ
10λ
20λ
40λ
60λ
THEORETICAL AND MEASURED PHASE VALUES
L = .185"
λg = 1.2774"
X = .186
λ = 1.2992"
z = 60λ
p = 13.04
z = 40λ
p = 8.69
z = 20λ
p = 4.35
z = 10λ
p = 2.17
z = 5λ
p = 1.09
20°
r ⟶
1" 2" 3" 4" 5" 6" 7" 8" 9" 10" 11" 12" 13" 14" 15"

FIGURE 10

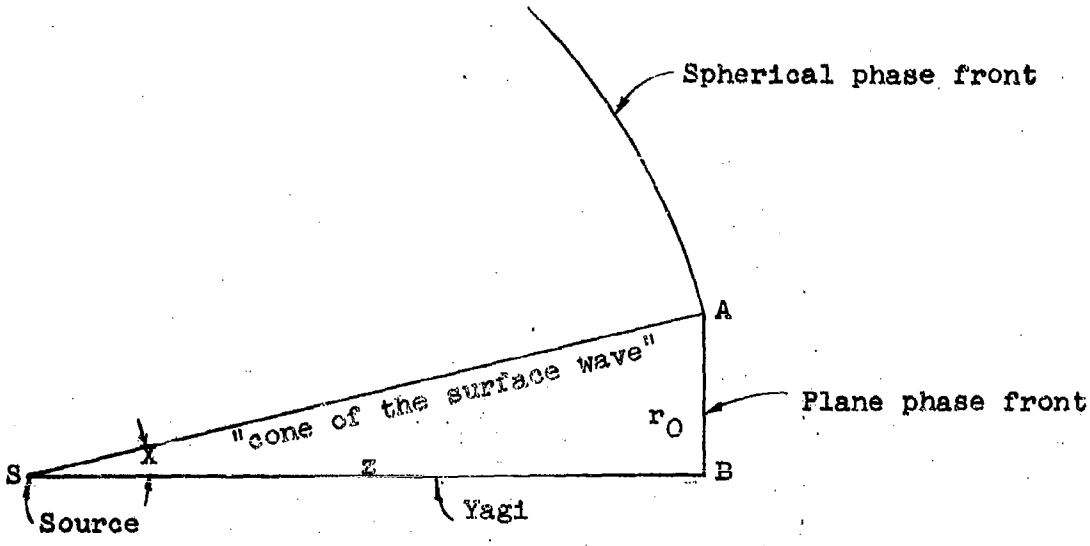

THEORETICAL PHASE FRONT SHOWING FLAT SURFACE WAVE PHASE FRONT SMOOTHLY JOINING SPHERICAL RADIATION FIELD PHASE FRONT AND RAYS FROM SOURCE

travels with free space wavelength, the energy on $\overrightarrow{SB}$ with wavelength λ_g. Hence

$$\frac{\sqrt{z^2+r_0^2}}{\lambda} = \frac{z}{\lambda_g} . \tag{16}$$

Since $\lambda/\lambda_g = \sqrt{1+X^2}$ this implies that

$$Xz = r_0 . \tag{17}$$

This is the equation of the "cone of the surface wave." The phase values which this theory implies are plotted for comparison with the measured curve in Figures 7, 8, and 9. Below values of $p = 4$, the agreement is quite good. At distances beyond $p = 4$, the phase front begins to break up at the surface wave, radiation field junction. At z distances where the

radiation field phase front appears to lead (lag) slightly the surface wave phase front, the radiation field phase front is retarded (advanced) and the surface wave phase front is advanced (retarded), so that the two tend to merge. However, when the two fields depart too far from each other in phase, there is a phase front discontinuity. The region where these effects take place has been called the "diffraction region."

VII. TOLERANCES

The effect of tolerances on the long yagis was most noticed in some of the phase front measurements. The pin height tolerances of ±.005" were about what was required for good measurements except for heights very close to the cut-off reactance (see Figure 6c). A tolerance of ±.010" was held in ground plane flatness on the first eight foot section and was also adequate. However due to an oversight, the last three eight feet long ground plane sections were of softer temper aluminum than the first section and lost their flatness in shipping. They contained many approximately-random ripples and bumps which departed from flatness by as much as ±.040". By holding the pin height tolerance the resulting yagi then undulated slightly as shown in Figure 11 in an exaggerated form.

FIGURE 11

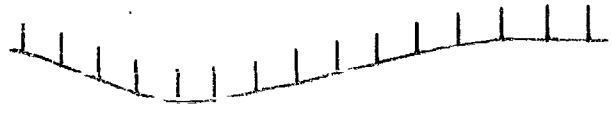

SCHEMATIC OF PINS ON "ROLLING" GROUND PLANE

The resulting effect on the surface wave was that it did not "fully" enter the ground plane valleys or "see" the pins "hidden" in them. As a result the effective reactance in these regions was reduced. On the "hills" the effective reactance was not changed. Over long path lengths, the net average reactance was accordingly less than its expected value. This situation is illustrated with the phase front measurement for a pin height $L = .144"$ at a great distance from the source. Figure 12 shows that at $z = 240\lambda$ the phase front fits fairly well a theoretical curve for the value of $X = .032$ (rather than $X = .040$ which was measured in the region $0 < z < 120\lambda$). At $z = 180\lambda$ the phase front fits the theoretical value for $X = .040$ very poorly. However, by increasing the pin heights by .020" in the interval $150\lambda < z < 180\lambda$, the undulating ground plane effect was compensated and the resulting phase front closely approached the theoretical value.

VIII. TRANSVERSE AMPLITUDE DEPENDENCE

From the measured values of X one may determine the theoretical amplitude dependence in any transverse plane from (10) as $K_0(kXr)$. These values were plotted and compared with measured values in Figures 13, 14, and 15. In Figures 13 and 14 the relative independence of these measured values with respect to θ are illustrated. We note again that measured values in the plane $\theta = 0$ are smoother. In Figure 15 the relative independence of the measured values with respect to z are illustrated.

FIGURE 12

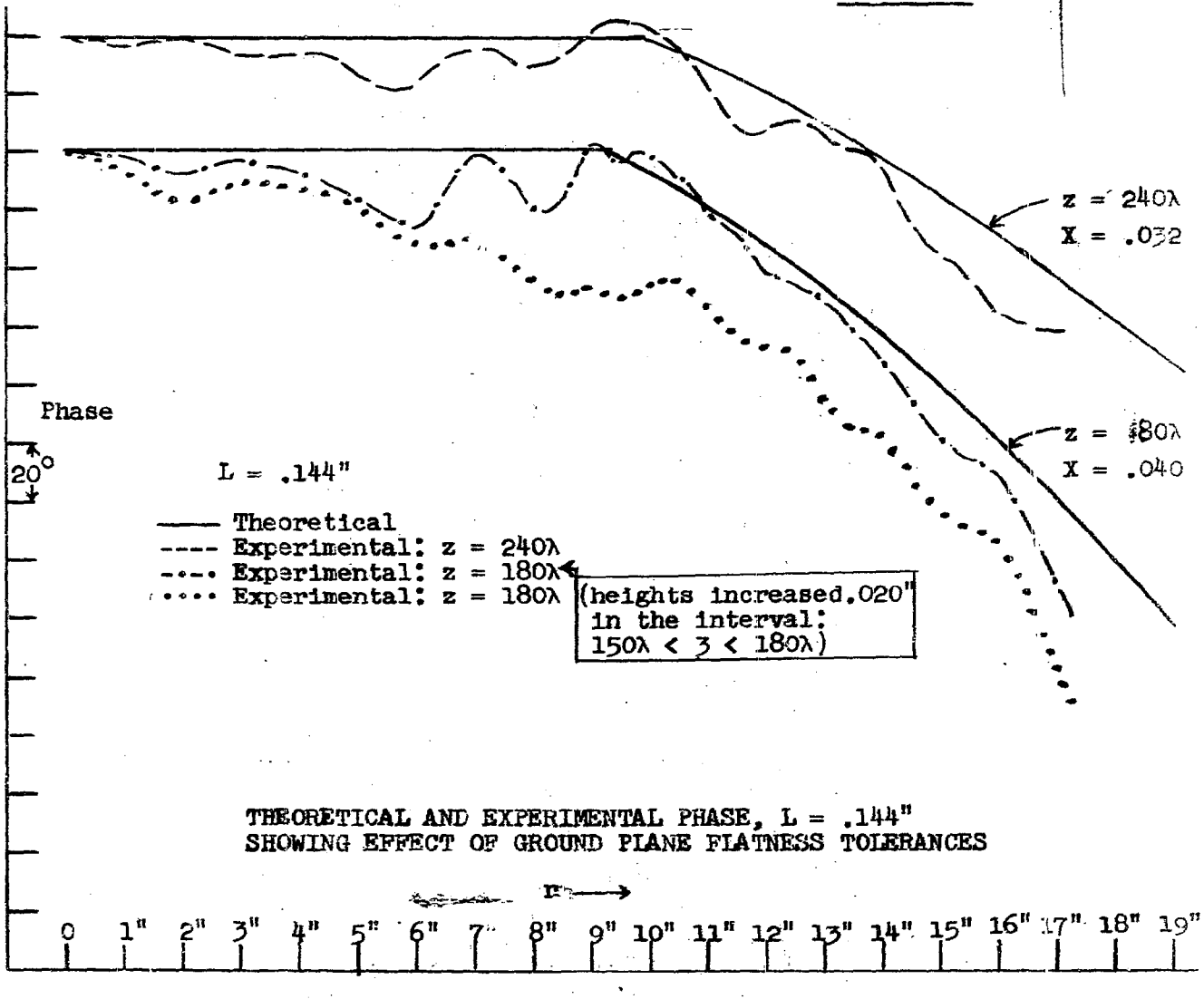

THEORETICAL AND EXPERIMENTAL PHASE, L = .144"
SHOWING EFFECT OF GROUND PLANE FLATNESS TOLERANCES

FIG. 13

L = .144"
z = 120λ
X = .040
p = 1.205

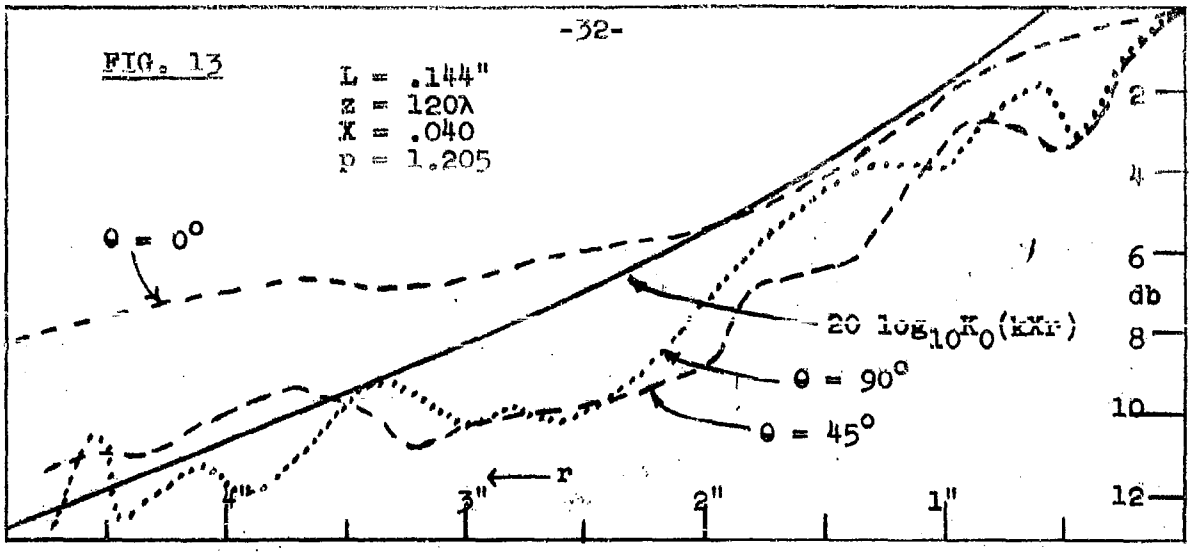

FIG. 14

THEORETICAL AND MEASURED
TRANSVERSE FIELD DECAYS

L = .169"
z = 70λ
X = .097
p = 4.14

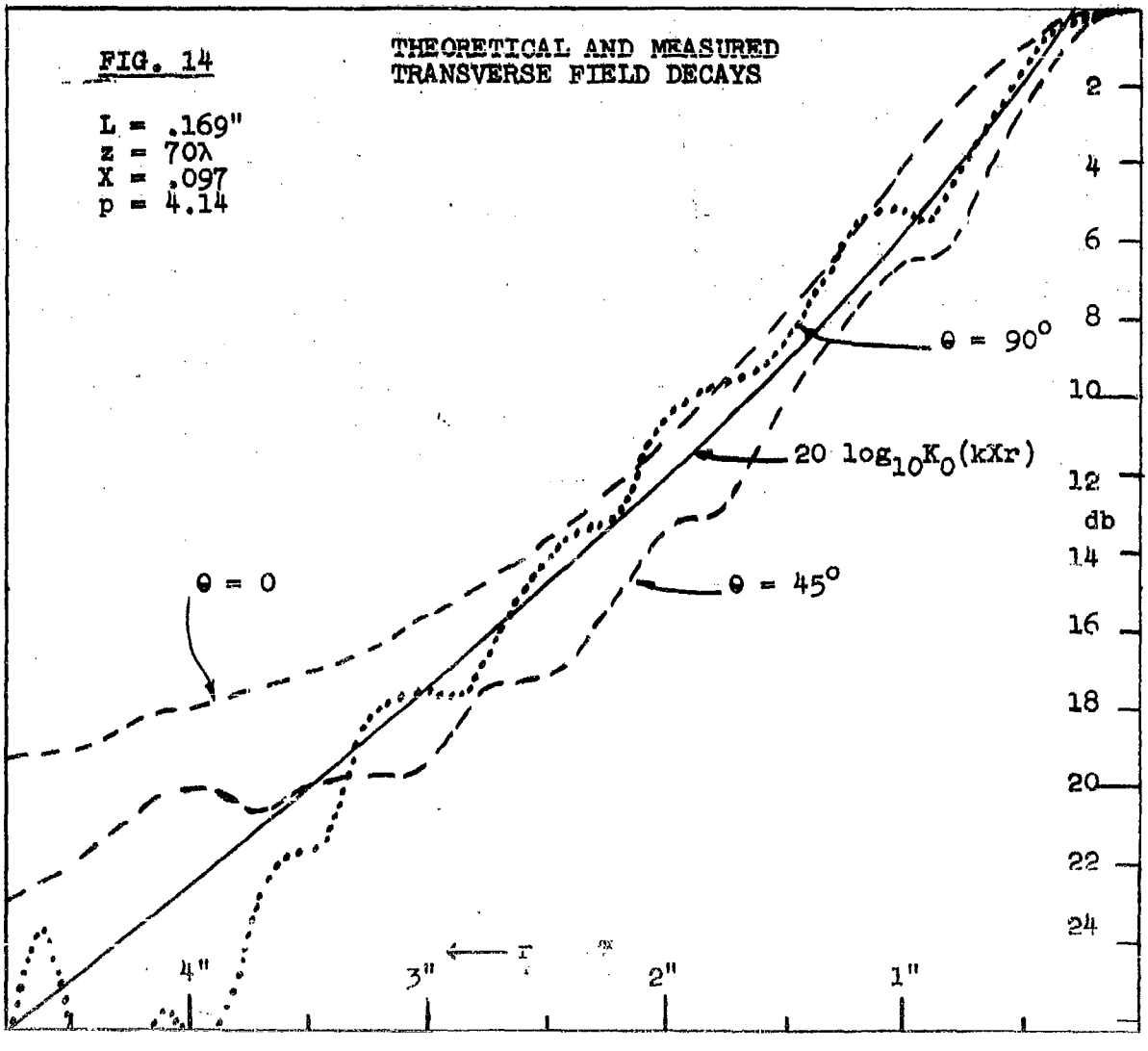

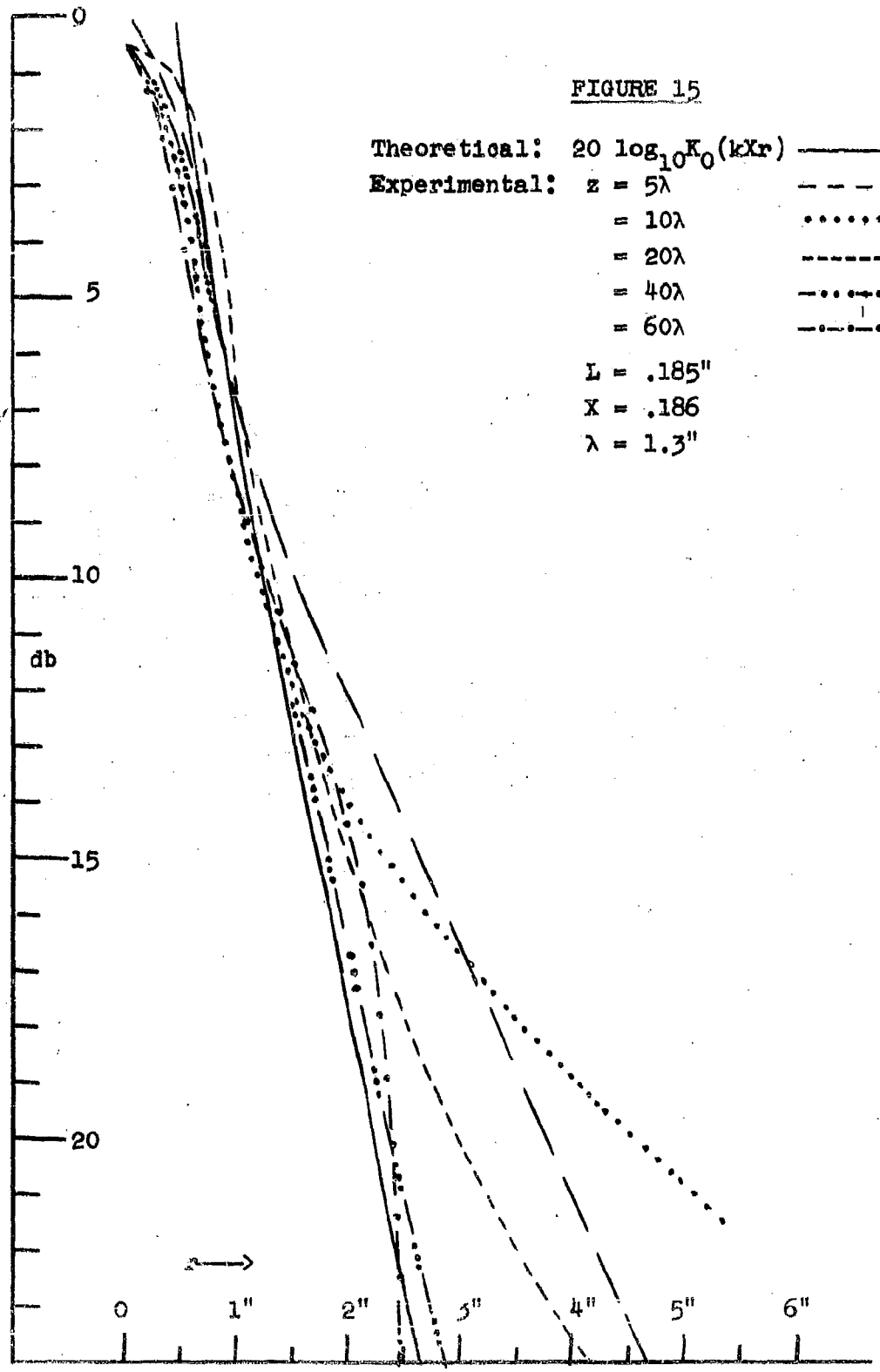

FIGURE 15

Theoretical: $20 \log_{10} K_0(kXr)$ ———

Experimental: z = 5λ – – – –

= 10λ ·····

= 20λ – – – – –

= 40λ —·—·—

= 60λ —·—·—

L = .185"

X = .186

λ = 1.3"

In the latter figure, all db values are with respect to a common reference. The good agreement here tends to confirm both the measured values of X and the theory of section (III).

IX. LONGITUDINAL AMPLITUDE DEPENDENCE

Results of measurements of the field amplitude dependence on z in the "cone of the surface wave" suggested a simple hypothesis: the surface wave energy is conserved. By this we mean that no energy crosses the cone from the radiation field to the surface wave or vice versa. As the wave travels along and spreads out in the cone, the energy in the wave spreads out too. If P(z) is the energy density of the surface wave at a fixed reference value of r, Poynting's theorem shows that the energy flow in the cone of the surface wave is proportional to

$$(18) \qquad P(z)\int_0^{Xz}\left[K_0(kXr)\right]^2 r\,dr = \frac{P(z)}{2k^2X^2}\left[1-p^2\left\{\left[K_1(p)\right]^2-\left[K_0(p)\right]^2\right\}\right]$$

where $K_0(p)$, $K_1(p)$ are the modified Hankel functions of the second kind. The surface wave energy conservation hypothesis is equivalent to the statement that (18) is independent of z, or

$$(19) \qquad P(z) = 10\log_{10}\left[1-p^2\left\{\left[K_1(p)\right]^2-\left[K_0(p)\right]^2\right\}\right]\text{db}.$$

This theoretical field variation is plotted versus the normalized distance parameter p in Figure 16. The measured values for L = .144 and .169 are also shown plotted vs p,

FIGURE 16

FIELD STRENGTH VS NORMALIZED DISTANCE ALONG THE YAGI

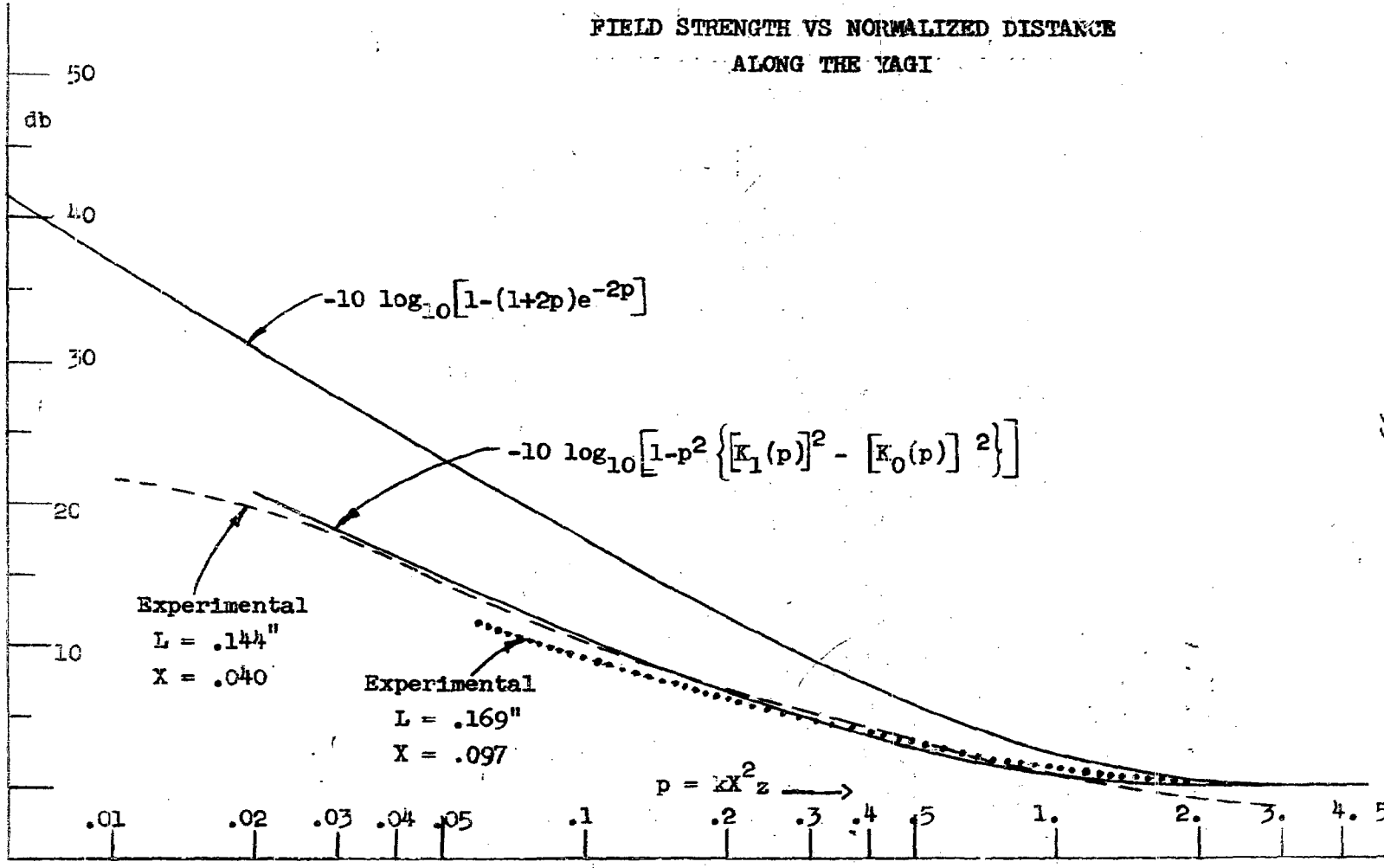

using the same values of X which agreed with the previous phase measurements and transverse amplitude measurements. We observe that at $p = 1$ the surface wave peak amplitude is within 1 db of its asymptotic value. In Figure 17, data taken from [2] for a 3λ yagi with $X = .45$ is also plotted vs p and compared to the theoretical curve. We believe that the good agreement between the theoretical and measured values places the theory on a secure footing.

In order to give some perspective to these results it is well to emphasize the great range in distance they encompass. For a short yagi with $\ell = 3\lambda$ and $X = .45$, the point $p = 1$ occurs at a distance of $.8\lambda$. The whole surface wave cone contains only about six pins. At the other extreme with $X = .040$, the full 32 feet of our yagi brings us only to $p = 3$. The data from $p = 1.5$ to $p = 3$ for this case, which appears relatively insignificant on the graph, required the use of the last 16 feet of the yagi with its 738 pins!

It may be of some interest to observe that for a time after it was first postulated we believed that the hypothesis of conservation of energy in the cone of the surface wave did not agree with the measured values. This came about because we assumed an exponential transverse field dependence, which is correct for a two-dimensional or fakir's bed structure, but is only an approximation to the modified Hankel function. This assumption leads to the equation

$$(20) \qquad P(z) = 10 \log_{10} \left\{ \int_0^{Xz} e^{-2kXr}\, r\, dr \right\} = -10 \log_{10} \left[1-(1+2p)e^{-2p} \right]$$

FIGURE 17

COMPARISON OF FIELD DECAY ALONG YAGI SURFACE MEASURED BY EHRENSPECK AND POEHLER [2] AND THEORETICAL DECAY PREDICTED BY EQ(19), "THE CONSERVATION OF SURFACE WAVE ENERGY."

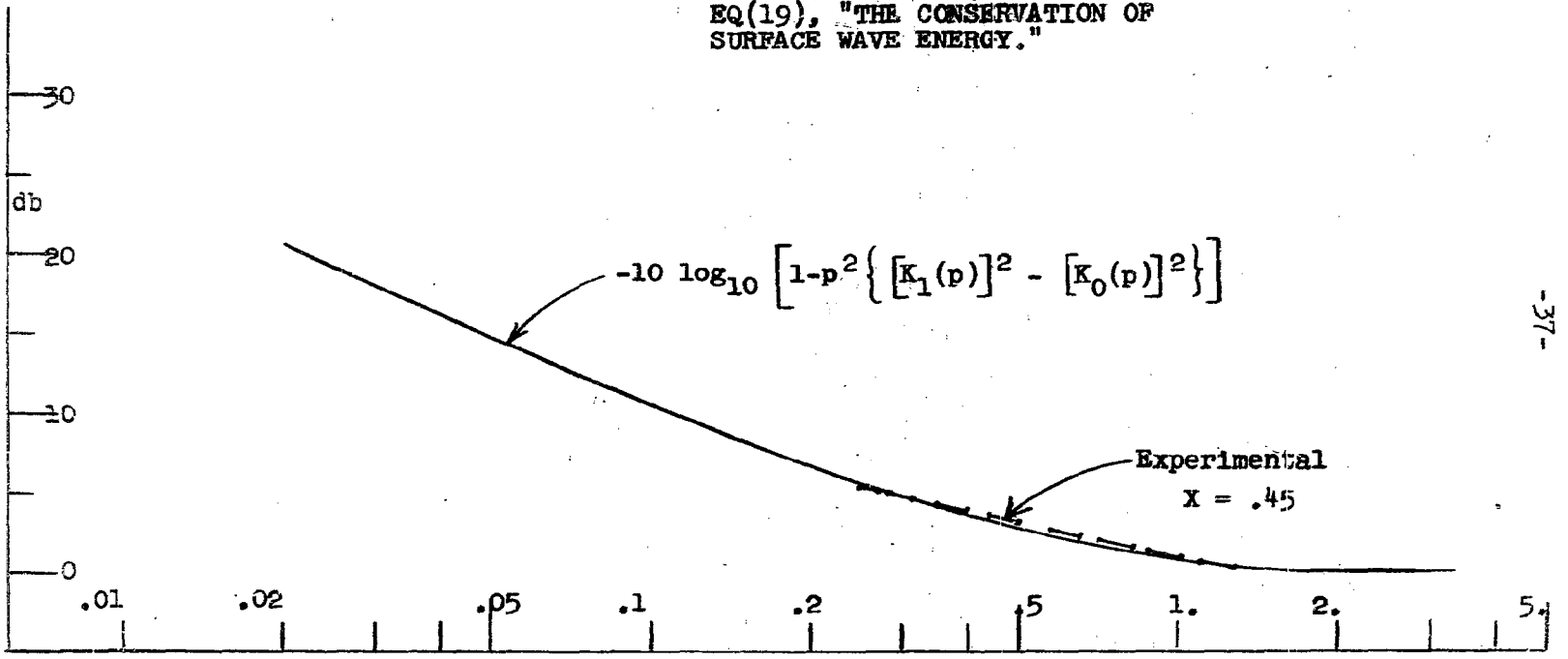

instead of (19). The poorness of fit of this expression as compared to (20) can be observed from Figure 16, and illustrates one of the significant differences between the yagi and the fakir's bed.

X. RADIATION FIELD

The spherical phase fronts of the radiation field region have been illustrated in Figures 7, 8, and 9. For amplitude plots in this region it is convenient to use a conventional (R,ϕ) polar coordinate system in the horizontal plane centered on the source, related to the previous coordinates by

(21) $$R = z \sec \phi, \quad r = z \tan \phi.$$

Figure 18 shows the measured field strength vs R for several values of ϕ for the case L = .185". For each value of ϕ, a theoretical inverse square dependence is also plotted. The boundary of the cone of the surface wave occurs at $\phi = 10.5^{\circ}$.

The variation of field amplitude across the boundary of the cone of the surface wave and the radiation field regions is very smooth. This could be generally anticipated from the conservation of surface wave energy hypothesis. From this hypothesis, the amplitude of the surface wave on the boundary ray $\phi = \tan^{-1}X$ is

$$10 \log_{10} \frac{K_0^2(p)}{1-p^2\left\{\left[K_1(p)\right]^2-\left[K_0(p)\right]^2\right\}}.$$

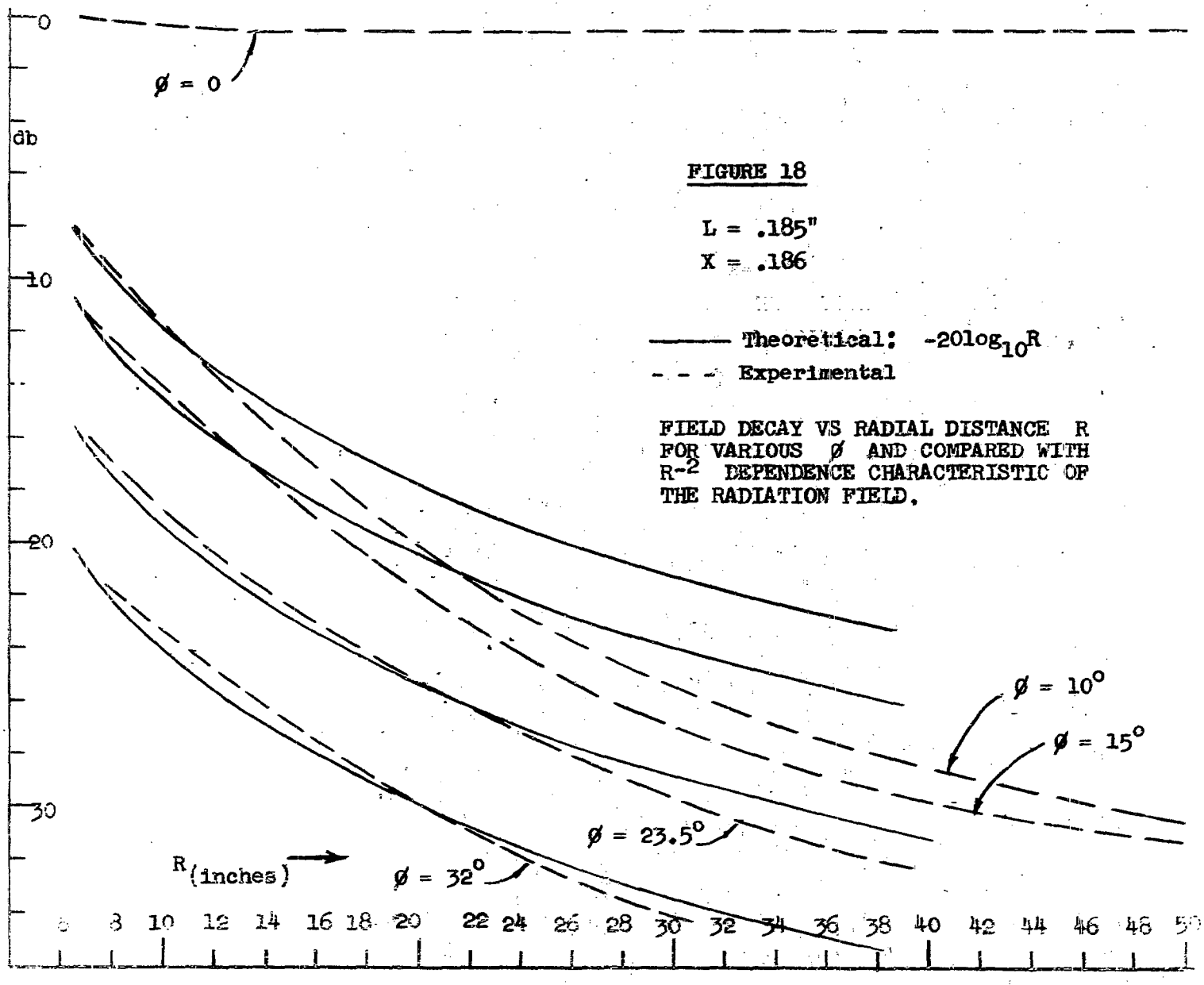

FIGURE 18

L = .185"
X = .186

——— Theoretical: $-20\log_{10}R$
- - - Experimental

FIELD DECAY VS RADIAL DISTANCE R FOR VARIOUS ø AND COMPARED WITH R^{-2} DEPENDENCE CHARACTERISTIC OF THE RADIATION FIELD.

This relation is plotted vs p in Figure 19 along with the inverse square radiation field dependence, $-20 \log_{10} p$. The two agree well for small values of p. For larger values of p, where they indicate an appreciable discontinuity, an abrupt variation is not observed in practice until at least $p = 2$, so that abrupt variations take place in the diffraction region. At $p \simeq 2\pi, 4\pi, \ldots$, there are definite field nulls across which the field changes in character from surface wave to radiation field with the 180° phase change previously mentioned. At other values of p the amplitudes of the two fields tend to pull each other into a smooth transition across the boundary of the surface wave region and the radiation or diffraction regions.

From Figure 18 one may also observe that the field angular pattern $P(\phi)$ in the radiation field region is somewhat narrower than the pattern of the same source in free space [11, p. 345] but the two are of generally the same character.

XI. CALCULATION OF FINITE LENGTH PLASER ANTENNA PATTERNS

The results of these investigations can be applied to the problem of the proper way to predict plaser far field patterns, a subject discussed at considerable length in [12]. Some confusion has been created by the possibility of predicting patterns in two different ways, either (a) by an integral over the PLASER itself or (b) by an integral over an "effective" aperture in a transverse plane at the termination of the PLASER. Of course, it must be possible to

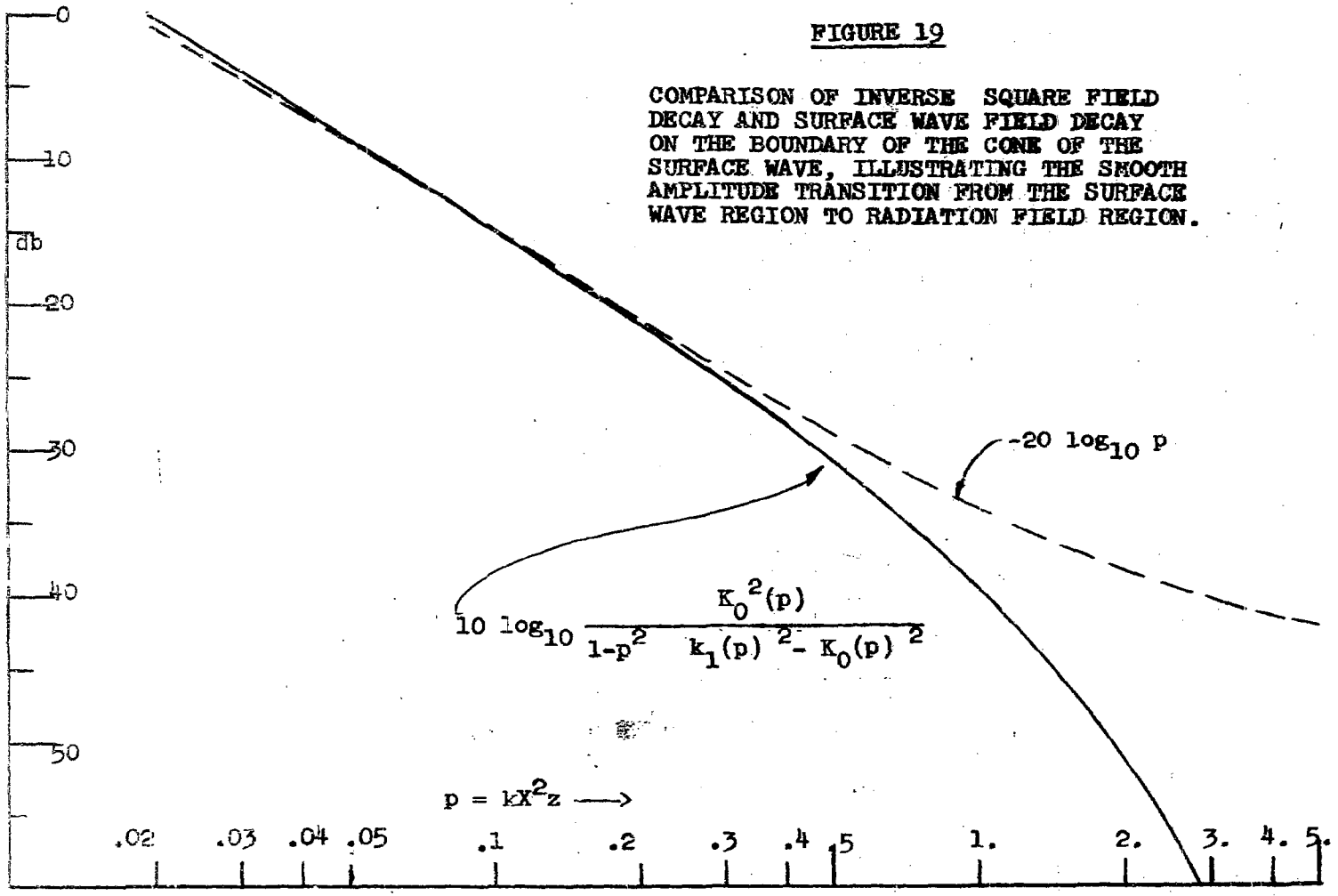

FIGURE 19

COMPARISON OF INVERSE SQUARE FIELD DECAY AND SURFACE WAVE FIELD DECAY ON THE BOUNDARY OF THE CONE OF THE SURFACE WAVE, ILLUSTRATING THE SMOOTH AMPLITUDE TRANSITION FROM THE SURFACE WAVE REGION TO RADIATION FIELD REGION.

successfully predict the pattern either way provided the correct sources and aperture fields are used. Determination of these correct values has been a considerable problem. It was stated in [12], for example, that only enough was known to predict patterns by method (b). We feel that now, perhaps, either method may be used.

In the case of method (a), if the correct non-uniform amplitude dependence is included, a reasonably good pattern should be obtained from simple line source pattern theory. The pattern would be given as a product of a dipole element factor times an array factor of the form

$$(22) \qquad P(\phi) = \sum_{n=0}^{N} a_n e^{j(w-\beta)nd}, \quad w = k \cos \phi$$

where from (19)

$$(23) \qquad a_n = \frac{1}{1-p_n^2\left\{\left[K_1(p_n)\right]^2-\left[K_0(p_n)\right]^2\right\}}, \quad p_n = kX^2nd, \quad n > 1 .$$

The coefficient a_0 corresponding to the strength of the feed itself would be infinite if defined by (23). Its correct value would have to be determined by other means. In addition, a term corresponding to a reflector element, if one is present, would also be required. However, we believe that for long plasers (22) should give a fairly good result even if these terms are omitted. In [2] it has been shown how the summation (22) with $w = k$ will predict the relationship of length to gain

of a yagi. The "a_n" values used in [2] were experimental, but we have shown (see Figure 17) that, for $n \geq 1$, they agree well with (23). There is no reason to believe that the entire pattern could not be predicted with equal success by the same formula with the more general value of w.

In case (b) we believe that if the yagi is terminated at the plane $z = \ell$ the far field pattern can be predicted from an integration over the "aperture plane" of the following form

$$P(\phi) = P_1 + P_2 \tag{24}$$

where

$$P_1 = \frac{e^{-j\beta\ell}}{\sqrt{1-p^2\left\{\left[K_1(p)\right]^2-\left[K_0(p)\right]^2\right\}}} \int_{S_1} K_0(kXr)e^{jur\cos\theta}\, r\, dr\, d\theta \tag{25}$$

$$P_2 = \int_{S_2} R(r,\theta)e^{jur\cos\theta}\, r\, dr\, d\theta, \quad u = k\sin\phi. \tag{26}$$

Here S_1 is a circle, the intersection of the plane $z = \ell$ and the cone (or, as the case may be, the cylinder) of the surface wave. The aperture field in S_1 is that of the pure surface wave. S_2 is the rest of the aperture plane, i.e. a plane with a hole removed, and the integration is over the radiation and/or diffraction field, denoted by $R(r,\theta)$, times the usual phase factor. P_1 may be evaluated explicitly in terms of cylinder functions by formulas given

in [12], p. 34.

We have no reliable general expression for $R(r,\theta)$. However, as an approximation, one might be tempted to assume the free space or radiation field of the feed alone. Our measurements have shown that this is a fairly good assumption at least if ℓ is small compared to λ/X^2. In this case we may let

$$R(r,\theta) = A\left[G(\phi,\psi)\right]^{1/2} \frac{e^{-jk\sqrt{\ell^2+r^2}}}{\sqrt{\ell^2+r^2}} \tag{27}$$

where $G(\phi,\psi)$ is the gain of the free-space source in direction (ϕ,ψ) the azimuth and elevation angles, respectively, given by

$$\psi = \tan^{-1}\left\{\frac{r \sin\theta}{\sqrt{\ell^2+r^2\cos^2\theta}}\right\} \tag{28}$$

$$\phi = \tan^{-1}\left\{\frac{r\cos\theta}{\ell}\right\}$$

and A is an amplitude coefficient chosen so that the radiation and surface wave fields are of equal amplitude across the S_1, S_2 boundary. The method in [12] is the same as this except that the integral in (26) is taken over the whole plane $z = \ell$, as a result of the implicit assumption made in [12] that the feed radiation field is present even near the yagi.

One can show that it is difficult to detect experimentally whether or not feed radiation field is present in the cone or cylinder of the surface wave. Suppose

for example that we assume that the field above a PLASER is given everywhere (except in the near field cylinder) by a pure surface wave plus a pure point source radiation field as follows:

$$(29) \qquad \frac{ce^{ik\sqrt{r^2+z^2}}}{\sqrt{r^2+z^2}} + K_0(kXr)e^{i\beta z}$$

where c is a constant chosen for the best fit with measured values. Such an assumption leads to the aperture fields used in [12].

A value of $c = .2K_0(kXr_0)/kX^2$, where $r_0 \simeq \lambda/2$, gives an excellent fit with the measured longitudinal field decay. (See Figure 20) Although we have not carried out detailed calculations, it seems likely that (29) would fit the measured amplitude and phase curves fairly well everywhere in space outside of the near field cylinder. We, therefore, are not in a position to offer direct evidence that (29) does not agree with measured values. The following indirect arguments make us feel that formulas (24)-(28) might predict more accurate patterns than the method given in [12].

1) The feed radiation field can not in fact exist near the yagi because it does not satisfy the yagi boundary conditions.

2) The agreement between the measured and theoretical patterns reported in [12] for one value of X ($\simeq .535$) and for a best-fitting value of c was good for a value of p of about 10.8 and

FIGURE 20

COMPARISON OF SURFACE WAVE LONGITUDINAL FIELD DECAY AS PREDICTED BY TWO DIFFERENT THEORIES:

——— eq.(19) "Conservation of Surface Wave Energy"

------ eq.(29) "Interference of Point Source and Pure Surface Wave."

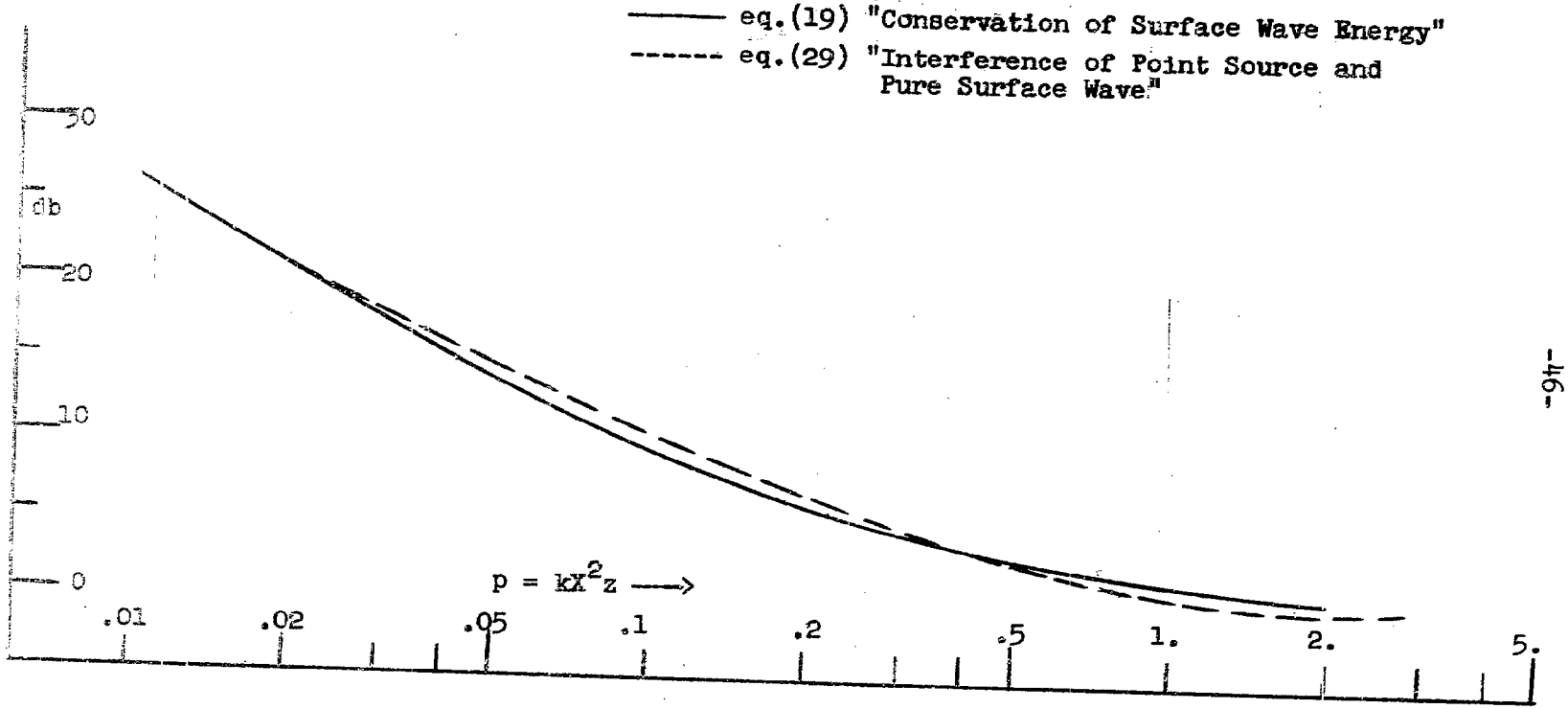

progressively poorer for smaller values of p. It can be shown that for large values of p, the two methods give almost the same results.

3) The method in [12] does not predict an optimum gain yagi for lengths near the Hansen-Woodyard

which is the Hansen-Woodyard condition.

Because our argument has involved several approximations, condition (31) should not be exact, and we know it is not. Only fairly tedious calculations based on (25) would show what optimum gain condition actually is predicted by that equation. However, this approximation argument has been given to show how an integration in the aperture plane can lead to a condition similar to the Hansen-Woodyard condition and take into account the feed radiation in a conceptually simple way.

XII. LIMITATIONS ON THE GAIN OF LONG YAGIS (CONCLUSION)

Our investigations, described above, have shown that at least for yagis up to 300λ in length, with proper care, ohmic losses and/or tolerances are not significant in limiting gain. For long yagis, it is true, that small tolerance errors, especially in the flatness of the ground plane, may accumulate to produce large phase errors leading to a poor pattern. However if during construction, the phase delay along the yagi is monitored, and the pin height increased or decreased accordingly so as to maintain the correct average and total phase delay over the length, large tolerance errors may be compensated for. A long yagi could probably be successfully built on a fairly uneven ground plane by this means.

Although this paper is concerned with uniform yagis, we do not wish to give the impression that we consider uniform pin height best either for gain or side lobe level. Investigations not reported here have shown that a stepped

or tapered design starting with a fairly large reactance ($X \simeq .4$) at the feed end and decreasing to a small value at the termination leads to better patterns than a long uniform reactance yagi of the same length. The case of the uniform PLASER has been treated in this paper because it is a simpler case which has not been well understood previously.

REFERENCES

1. Elsasser, W.M., "Attenuation in a Dielectric Circular Rod," J.A.P., Vol. 20, p. 1193, 1949.
   Chandler, C.H., "An Investigation of Dielectric Rod as Waveguide," J.A.P., Vol. 20, p. 1188, 1949.

2. Ehrenspeck, H.W., Poehler, H., "A New Method for Obtaining Maximum Gain from Yagi Antennas," Antenna Laboratory, AFCRC, Bedford, Mass., ERD-CRRDA-TM-56-123.

3. Simon, J.C., Biggi, V., "Un Nouveau Type d'Aerien et Son Application a la Transmission de Television a Grande Distance," L'Onde Electrique, Vol. 332, pp. 3-16, November 1954.

4. Hansen, W.W., Woodyard, J.R., "A New Principle in Directional Antenna Design," Proc. of I.R.E., Vol. 26, No. 3, pp. 333-345, March 1938.

5. Dolph, C.L., "A Current Distribution of Broadside Arrays which Optimizes the Relationship Between Beam Width and Side Lobe Level," Proc. I.R.E., Vol. 35, pp. 489-492, May 1947, also Vol. 34, pp. 335-348, June 1946.
   Riblet, H.J., "Discussion on a Current Distribution for Broadside Array which Optimizes the Relationship Between Beam Width and Side Lobe Level," Proc. I.R.E., Vol. 35, No. 5, pp. 489-492, May 1947.

6. Kay, A.F., "Scattering of a Surface Wave by a Discontinuity in Reactance," TRG, Inc., AFCRC-TN-56-778, September 1957; PGAP, AP-7, January 1959, p. 22.

7. Oliner, A.A., "Equivalent Circuits for Slots in Rectangular Waveguide," AF19(122)-3, August 1951, p. 130.

8. Sommerfeld, A., "Partial Differential Equations in Physics," New York Academic Press, 1949.

9. Storer, J.E., Sheingold, L.S., and Stein, S., " A Simple Graphical Analysis of a Two-Port Waveguide Junction," Proc. I.R.E., Vol. 41, p. 1004, 1953.
   Deschamps, G.A., "Determination of Reflection Coefficients and Insertion Loss of a Waveguide Junction," J.A.P., Vol. 24, p. 1050, 1953.

10. Reynolds, D.K., "Broadband Travelling Wave Antennas," I.R.E. Convention Record, Antennas and Propagation, p. 99, 1957.

11. Silver, S., "Microwave Antenna Theory and Design," Radiation Lab. Series, Vol. 12, McGraw-Hill, New York, 1949.

12. Brown, J., Spector, J.O., "The Radiating Properties of End-Fire Aerials," J.I.E.E., Part B, Vol. 104, pp. 27-32, January 1957.

Master Distribution List for Antenna Laboratory Reports LIST S-S

List Identifiers:

1a	Ground Navigation Antennas
1b	Airborne Navigation Antennas
2a	Ground Communication Antennas
2b	Airborne Communication Antennas
3a	Ground Radar Antennas
3b	Airborne Radar Antenna
4a	Ground E.C.M. Antennas
4b	Airborne E.C.M. Antennas
5	General Antenna Research
6	Radar Reflections
7	Antenna Materials Research

Note: (a) One copy unless otherwise designated
(b) Addressee will receive reports on all above categories unless otherwise indicated.

CODE	ORGANIZATION	LIST (if other than all)
AF 15	ARDC (RDSPE-3) Andrews AFB, Wash 25, D. C.	3a, 3b, 4a, 4b and 6 only
AF 29	AFGC (PGTRI, Tech Lib) Eglin AFB, Fla.	
AF 69	Director of Resident Training 3380th Technical Training Group Keesler AFB, Mississippi Attn: OA-3011 Course	
AF 18	AUL Maxwell AFB, Ala.	
AF 86	SAC (Operations Analysis Office) Offutt AFB, Nebraska	
AF 5	AF Missile Test Cen Patrick AFB, Fla. Attn: MTGRY (For classified documents) Attn: AFMTC, Tech Library, MU-135 (for unclassified documents)	
AF 227	USAF Security Service (CLR) San Antonio, Texas	
AF 28	Hq. USAF (Major R.L. Stell) Tactical Air Group Wash 25, D. C.	

Code	Organization	List (if
AF 91	AFOSR (SRY, Mr. Otting) 14th Street and Constitution Avenue Washington, D. C.	
AF 166	Hq. USAF (AFOAC-S/E) Communications-Electronics Directorate Wash 25, D. C.	
AF 63	WADD (WCLRSA) Attn: Mr. Portune Wright-Patterson AFB, Ohio	
AF 43	WADD (WCLJA-2) Attn: Aeronautical Research Lab. Res. Div. Wright-Patterson AFB, Ohio	
AF 65	WADD (WCLNI-A) Attn: N. Draganjac Wright-Patterson AFB, Ohio	
AF 68	WADD (WCLRE-5) Attn: Mr. Paul Springer Wright-Patterson AFB, Ohio	5, 6 an
AF 231	Director, Electronics Division Air Technical Intelligence Center Attn: AFCIN-4El, Colonel M.K. Gilbert Wright-Patterson AFB, Ohio	
AF 141	WADD (WCLJH) Attn: Dr. C.A. Trexler Wright-Patterson AFB, Ohio	5 and 7
AF 142	WADD (WCRTR-4) Attn: D.H. Cartellano Wright-Patterson AFB, Ohio	1a, 2a, only
AF 124	RADC (RCSSTL-1) Griffiss AFB, N.Y.	
AF 120	RADC (RCUE) Attn: Mr. Donald Dakan Griffiss AFB, N.Y.	
AF 143	RADC (RCE) Attn: Dr. John S. Burgess Griffiss AFB, N.Y.	5 only
AF 139	AF Missile Dev. Cen. (MDGRT) Attn: Technical Library Holloman AFB, New Mexico	1a and emitte